Cambrian Age 3 small shelly fossils from the Terrades inlier, southern Pyrenees, Spain: Biostratigraphic and paleobiogeographic implications

Elise Wallet, Maxime Padel, Léa Devaere, Sébastien Clausen, J. Javier Álvaro, Bernard Laumonier

Cambrian Age 3 small shelly fossils from the Terrades inlier, southern Pyrenees, Spain: biostratigraphic and paleobiogeographic implications

Elise Wallet[1,3], Maxime Padel[2], Léa Devaere[3,4], Sébastien Clausen[3], J. Javier Álvaro[5], Bernard Laumonier[6]

[1] Department of Earth Sciences, Palaeobiology, Uppsala University, Villavägen 16, 752 36 UPPSALA, Sweden <elise.wallet@geo.uu.se>

[2] Bureau de Recherches Géologiques et Minières (BRGM), 23 Avenue Claude Guillemin, 45100 Orléans, France <m.padel@brgm.fr>

[3]Univ. Lille, CNRS, UMR 8198 - Evo-Eco-Paleo, F-59000 Lille, France <sebastien.clausen@univ-lille.fr> <lea.devaere@univ-lille.fr>

[4] Museum für Naturkunde, Leibniz Institute for Evolution and Biodiversity Science, Berlin, Invalidenstraße 43, 10115 Berlin, Germany

[5] Instituto de Geociencias (CSIC-UCM), Dr. Severo Ochoa 7, 28040 Madrid, Spain <jj.alvaro@csic.es>

[6] École des Mines de Nancy, GeoRessources, UMR 7359, Université de Lorraine, Campus ARTEM, CS14234, 54042 Nancy Cedex, France <blaumonier@wanadoo.fr>

Abstract.— The Cambrian stratigraphic succession of the Pyrenees (SW Europe) has undergone a complex Variscan and Alpine tectono-thermal history leading to marked

metamorphism and development of cleavage networks, which might partly explain the lack of Cambrian fossiliferous beds. This gap has traditionally precluded its paleobiogeographic and biostratigraphic relationships with other neighboring peri-Gondwanan units. Correlations are only based on lithostratigraphic comparisons and radiometric constraints. In this general scheme, the Terrades inlier (Gerona Province, Spain) provides the only significant and indisputable "early Cambrian" fossil record of the Pyrenees. This outcrop had so far yielded archeocyaths dated at Cambrian Epoch 2, Age 3. This paper describes, for the first time, the microfossil assemblage included in the archeocyathan-microbial reefal complex that crops out in the Terrades inlier in order to precise its affinities with surrounding tectonostratigraphic units. Reefal flanks of patch-reefs have yielded bradoriids, brachiopods, molluscs, tommotiids, chancelloriids, hyoliths and the problematic fossil (and chronostratigraphically significant) *Rhombocorniculum cancellatum*. Moreover, this study emphasizes strong faunal affinities with the surrounding Occitan Domain (Montagne Noire, southern Massif Central, France) and Sardinia (Italy). Along with lithostratigraphic comparison and tectonic considerations, this further supports the recent reconstructions positioning the Pyrenean domain between the Montagne Noire (to the west) and Sardinia (further to the east) on the Gondwana margin during Cambrian times.

Introduction

The Variscan Ibero-Armorican Arc comprises two branches that represent two Cambrian lateral margins of West Gondwana (Pouclet et al., 2016) (Fig. 1): the SW branch comprises the Iberian Massif, and the NE branch the Armorican Domains, the northern Massif Central, the Occitan

Domain (or southern Massif Central, including the Montagne Noire) and its lateral equivalent through southern Corsica and Sardinia, and the Pyrenean Domain. In the Pyrenees, the Ediacaran–Lower Ordovician (pre–Sardic) stratigraphic succession is laterally variable owing to structural complexity and related metamorphism. As a result, the radiometrically controlled Cambrian deposits are variously affected by the Variscan metamorphism and, except two single findings of poorly preserved acritarchs (Laumonier et al., 2015; Casas and Palacios, 2012), mostly depleted of fossil record (Perejón et al., 1994; Laumonier et al., 1996, Padel et al., 2017, 2018b; Casas et al., 2019). Nevertheless, the Ediacaran–Cambrian lithological successions of the eastern Pyrenees share close similarities with those from the Iberian Chains and the Cantabrian Zone (Spain), the Montagne Noire (France) and SW Sardinia (Italy), supporting reliable lithostratigraphic correlations (Laumonier et al., 1996, 1998, 2004; Padel et al., 2018b). In the eastern Pyrenees, some volcanosedimentary complexes have been recently constrained by U–Pb zircon dating, in which the Ediacaran–Cambrian boundary interval has recently been precisely identified (Padel et al., 2017, 2018a). However, while paleo(bio)geographic relationships between most of the Cambrian domains of the Ibero-Armorican Arc are now relatively well established (~~see~~ e.g., Álvaro et al., 2010, 2021; Pouclet et al., 2016), the Cambrian setting of the tectonostratigraphic Pyrenean subunits remains uncertain (Laumonier et al., 1996, 2004; Ballèvre et al., 2009; Álvaro et al., 2014a; Pouclet et al., 2016). As a result, the paleogeographic position of the Pyrenees is often questioned or even omitted in many Ediacaran–Early Paleozoic paleogeographic reconstructions of Gondwana (e.g., Murphy et al., 2004; Nance et al., 2008; but see Álvaro et al., 2010; Pouclet et al., 2016).

The Terrades inlier, located in the southeastern Pyrenees (Gerona province, Spain) (Fig. 2), stands apart from this general scheme. It has provided the only significant and indisputable early Cambrian fossil record from the Pyrenees. Broad correlations between the Terrades inlier and the Iberian Peninsula, Morocco, Siberia, Sardinia, China and Montagne Noire have been

suggested based on the described Cambrian Epoch 2, Age 3 archeocyaths (late Ovetian according to the Iberian chart, and early Botoman according to the Siberian chart; Abad, 1988; Perejón et al., 1994; Laumonier et al., 1996; Menéndez et al., 2015). The presence of skeletonized microfossils, usually known as 'Small Shelly Fossils' (*SSF*), have been mentioned from the described reefal and peri-reefal deposits, but never formally studied (Abad, 1988; Perejón et al., 1994). Cambrian small shelly fossils are highly common and diverse worldwide in earliest Cambrian carbonate platforms and have been therefore intensely studied for their major chronostratigraphic and paleobiogeographic implications (Devaere et al., 2013; Babcock et al., 2014; Clausen et al., 2015; and references therein).

This paper is aimed at describing for the first time the SSF assemblage from the Terrades inlier in order to further assess advanced correlations of the pre–Variscan successions in the Pyrenees, and in particular to precise the paleobiogeographic affinities between the Pyrenees and neighboring areas of West Gondwana.

Geologic setting

The Pyrenean Ranges (France-Spain), bounded by the North- and South-Pyrenean fault Thrusts, is structurally subdivided into three major E–W-trending zones (Barnolas et al., 1996): the Northern, Axial and Southern zones (Fig. 2). The Ediacaran–Cambrian sedimentary record of the Pyrenees mainly crops out in the eastern part of the range, from the Mediterranean Sea to the Noguera-Pallaresa valley. The eastern Axial Zone mostly consists of Ordovician (Sardic-related) and Variscan granitic intrusions encased in a thick Ediacaran–Ordovician sedimentary succession that was consequently affected by polyphasic metamorphic and deformation events (Olivier et al., 2008; Laumonier et al., 2004, 2010; Aguilar et al., 2014; Denèle et al., 2014;

Pereira et al., 2014; Cochelin et al., 2017, 2018; Lemirre et al., 2018). The Southern Pyrenean Zone, where the Terrades inlier is located (Figs. 2-3), mostly consists of Paleogene successions interrupted by Mesozoic klippes. The Souhern Pyrenean Zone overthrusts, through the South-Pyrenean Fault, the variably deformed strata of the Cenozoic Ebro Foreland Basin.

The Ediacaran–Lower Paleozoic stratigraphic scheme of the Pyrenees was defined based on the successions cropping out in the Axial Zone (Cavet, 1957; Laumonier et al., 1996, 2004). It has traditionally been divided into the Ediacaran Canaveilles Group and the Cambrian–Lower Ordovician Jujols Group (Fig. 4), recently revised by Padel et al. (2018). The Canaveilles Group consists of a heterogeneous set of shales and marbles with tuffs and volcano-sedimentary complexes which record the Ediacaran–Cambrian transition (Padel et al., 2018a). The siliciclastic Err Formation forms the lower part of the Jujols Group; it is overlain by the Valcébollère Formation, which consists of massive carbonates overlain and grading laterally into shale/carbonate alternations and green shales bearing carbonate nodules. This formation is estimated to be Cambrian Age 3–early Age 4, according to the local occurrence of acritarchs reported by Laumonier et al. (2015). As a consequence, the Ediacaran–Cambrian succession of the Axial Zone has been traditionally compared to the chronostratigraphically constrained and lithologically similar successions from the Montagne Noire (southern France; Cavet et al., 1957; Laumonier et al., 1996; Álvaro et al., 2014a; Padel et al., 2018a) (Fig. 4). In addition, the Ediacaran–Cambrian boundary has been geochronologically constrained in both areas using U–Pb dating of zircon of volcanosedimentary rocks (Padel et al. 2017, 2018a).

The Terrades inlier (also referred to as La Salut unit; Laumonier et al., 2004; Baudin et al., 2008; Padel et al., 2018b) is a stratigraphic exception because its involved Cambrian limestones (not marbles) display detailed textural features that are absent in the time-equivalent Valcebollère Formation. The inlier is located in the southern zone, near Figueres (Gerona

province) (Fig. 3). The Cambrian carbonate rocks of the Terrades inlier crop out in two places (Abad, 1988; Perejón et al., 1994): near Can Vila de Subirats (F11 section in Perejón et al., 1996) and along the road GI-504 from Terrades to Boadella (F12-F13 sections in Perejón et al., 1996). The succession outcropping near Can de Vila de Subirats is dominated by limestone strata, whereas the outcrop aside and below from the GI-504 is siliciclastic-dominated but containing archaeocyathan-microbial patch-reefs. The latter can be further subdivided into two outcrops located on the right and left banks of the Salt del Barral stream underlying the GI-504 road. The left bank (F12 section in Perejón et al., 1996) presents metre-sized calcimicrobial reefs overlain by decimetre archeocyath-microbial patch-reefs surrounded by onlapping shales (Fig. 5). The right bank is siliciclastic-dominated and contains decimetre-sized archeocyath-microbial patch-reefs at its base.

Material and methods

Samples were recovered from the left bank of the Salt del Barral stream close to the GI-504 road (F12 section in Perejón et al., 1996; localization: 42°19'17.30"N; 2°50'42.20"E; Fig.3). Most samples were extracted from flanks onlapping archeocyathan-microbial patch-reef cores (Fig. 5), preserved as limestones and not as marbles. Phosphatized microfossils were etched from their carbonate matrix through maceration in c. 10% acetic acid. Acid solution was renewed and residues sieved (using 50 μm, 100 μm, 250 μm, 1 mm and 2 mm meshes) every 48 hours. Microfossils were hand-picked from the dried residues under binocular microscope. Specimens were pictured using a Scanning Electron Microscope (SEM) FEI Quanta 200 at the Oceanography and Geosciences laboratory (LOG, UMR 8187 CNRS) of the University of Lille I, France.

Repositories and institutional abbreviations.— All specimens are housed in the paleontological collections of the University of Lille (acronym USTL).

Systematic paleontology

Phylum ARTHROPODA Siebold and Stannius, 1845

Class uncertain

Order BRADORIIDA Raymond, 1935

Family, genus, species uncertain

Remarks.— Bradoriids are described below following the terminology of Siveter and Williams (1997), Hou et al. (2001) and Vannier et al. (2005). They are oriented according to the criteria given by Hinz-Schallreuter et al. (2007): when present, the dorsal cusp and/or the oblique ridge between one node and the dorsum are considered anterior.

Specimens recovered herein are deformed with crinkled valves (Fig. 6.1, 6.13, 7.5, 7.9, 7.19, 7.10), which is consistent with a flexible, weakly mineralized to unmineralized shield construction, which would have been secondarily phosphatized (Siveter and Williams, 1997; Vannier et al., 2005; Zhang et al., 2007; Devaere et al., 2014b).

Bradoriid sp. A

Figure 6

Material.— One articulated specimen, broken ventrally, preserved as phosphatized carapace (USTL XX).

Occurrence.— Sample TE2F.

Description.—The valves are ~1.12 mm in length and ~741 μm in width, with a L/H ratio ~1.5. The anterodorsal spine is ~362 μm in length. The carapace is constituted of two valves articulated at the dorsum. The subamplete valves are connected through a well-defined hinge line anteriorly interrupted to form a faint cusp (Fig. 6.1-2). No cardinal spines are observed. The lobation consists of a slightly developed posterodorsal lobe, subparallel to the dorsal margin, extending from below the anterior cardinal corner to about one third the length of the valve. The weak anterodorsal lobe is prolonged by an elongated spine (Fig. 6.4-5), inclined anteriorly and bent toward the ventral margin at mid-height (the orientation may be taphonomically constrained; Fig. 6.2-3). Its base is extended ventrally into a narrow, well-defined ridge extending to the mid-length of the valve (Fig. 6.1-2). Admarginal ridges and furrows are absent. The surface does not show any other ornamental feature.

Remarks.— The lack of diagnostic features precludes a definite assignment for this specimen at the family level. Non-diagnostic spines are present in a number of bradoriid species (Topper et al., 2013). However, their overall shape, size and location strongly differ from the prominent, elongated anterodorsal spine observed on the specimen studied herein. Its curvature toward the ventral margin seems to be taphonomically constrained ~~origin~~, given the crinkle line observed in ventral view (Fig. 6.3). A similar anterodorsal spine connected to a ventrally extending ridge is also found in the monasteriid *Monasterium oepiki* Fleming, 1973, yet it is of Miaolingian age and lacks posterior lobe and cusp (Hinz-Schallreuter, 1992; Topper et al., 2013). An anterodorsal cusp characterizes only two bradoriid families, the Cambriidae and Kunmingellidae (Hou et al., 2001; Williams et al., 2006). However, both of them show extremely short cardinal spines or prominent ventral spines (e.g., *Kunmingella typica* Huo and

Shu, 1985, Hou et al., 2001). Nonetheless, some enigmatic genera showing elongate spines in the cardinal area were tentatively assigned to those families (e.g. *Isoxys* Walcott, 1890 and *Gladioscutum* Hinz-Schallreuter and Jones, 1994, Siveter et al., 1996; Vannier et al., 2005). Their extremely fine and elongated shape is nonetheless absolutely different from what is observed on the specimen herein.

Family CAMBRIIDAE? Lee, 1975

Bradoriid sp. B

Figures 7-9

Material.—About 30 articulated valves, more or less fragmentary, preserved as phosphatized valves and/or phosphatic internal molds, including the figured specimens USTL XX-XX.

Occurrence.— Sample TE2F.

Description.— The valves range from 679 μm to 2.4 mm in length, and from 338 μm to 1.6 mm. in height; the L/H ratio ranges from 1.22 to 2. The maximum length of the ornamentation spines is ~25 μm, and their maximum diameter ~35 μm. The carapace is constituted of two valves articulated at the dorsum. The orientation is inferred after the presence of a faint to well developed, ridge-like swelling between a node and the dorsum which is considered as the antero-dorsal ridge (arrowed in Fig. 7). The valves are amplete (Figs. 7.1, 7.5, 7.10, 8.14, 9.6-7, 9.10) to weakly preplete and elongate (Figs. 7.2, 8.1, 8.8, 8.21, 9.1). The hinge line is well defined, straight (Figs. 7.3, 7.6, 7.10, 7.13, 8.2, 8.4, 9.1) to faintly curved dorsally (Figs. 7.1, 8.1) and slightly shorter than or equal to the length of the valve. The ventral margin is rounded anteriorly, with dorsal extremities approximately perpendicular to the dorsal margin, forming nearly right cardinal corners (Figs. 7.1-2, 7.11, 7.13, 8.1, 8.7). The cardinal corners,

when preserved, have short cardinal spines (Figs. 7.1-4, 7.10-11, 7.13, 8.21). The lateroadmarginal ridge is often missing (damaged?), although better preserved specimens show a discrete to well developed, lateroadmarginal broad swelling of the ventral margin (Figs. 7.4, 8.1, 8.8, 8.17, 9.7, 9.9), in some cases bordered ventrally by a narrow flat strip (Figs. 8.3, 8.17, 9.7, 9.9). The anterodorsal and posterodorsal nodes are strongly convex, rounded, boss-like (Figs. 7.1-2, 7.6, 8.1, 8.11, 8.14, 8.19, 8.21, 9.1, 9.6-7) to ridge-like (Figs. 7.9, 7.11, 7.13, 8.4, 8.8), and run from cardinal regions to about mid-height of the valve. They are conjoined ventrally by a slightly narrower connecting the ridge, which tends to reduce or even become faint at mid-length (Figs. 7.2-6, 7.10, 7.13, 8.1, 8.17). The maximum elevation of nodes is reached toward the cardinal corners (Figs. 7.4, 7.11, 7.13, 8.3-4, 8.8, 8.14). The anterodorsal node tends to be slightly better developed (Fig. 7.2-6). The antero-dorsal ridge is a faint to well developed, ridge-like swelling emerging dorsally to or from the anterodorsal node and run obliquely to about the mid-dorsal area (Fig. 7.2, 7.6, 7.12, 7.14). On the exterior side of the anterior and posterior nodes, a large, broadly spaced pustulose to spiny ornament (often distally abraded) tends to be distinct (Figs. 7.2-3, 7.5-8, 7.13, 8.4, 8.6-9), but covers the entire surface of the valve in better preserved and larger specimens (Figs. 7.13-15, 8.14, 8.17, 8.19, 8.21). A polygonal surface ornament may be observed on thin layers overlying the spinose ornament (Figs. 7.8, 8.14-16, 8.19-20, 9.5). Smaller specimens (Fig. 9) have a slightly different aspect. One specimen preserved as internal mold exhibits a clear straight hinge line (Fig. 9.1-2). Otherwise, the phosphatized small specimens have a faint to absent connecting ridge and their surface is smooth, except by a fine ornament of polygonal ridges visible on one anterior node (Fig. 9.5).

Remarks.— The mixture of diagnostic features from different families precludes any definite assignment of the material at the family level. The present specimens exhibit some diagnostic features of the family Cambriidae (see Siveter et al., 1996, Hou et al., 2001, Williams et al.,

2006), such as the presence of two subcircular to elongate ovate nodes, a ventrally situated narrow to broadarcuate connecting ridge (except in smaller specimens), a lateroadmarginal ridge between the cardinal corners and a granular outer surface (see Siveter et al., 1996; Hou et al., 2001; Williams et al., 2006; Hinz-Schallreuter et al., 2007). A pustulose ornamentation, more developed on the lobes, and the presence of an anastomosing network of fine ridges on lateral surface, along with the presence of an antero-posterior ridge emerging from the lobe, are further distinct characters of the family, although not diagnostic (Hou et al., 2001; Hinz-Schallreuter, et al., 2007). Striking similarities can be pointed out with the genus *Cambria* Neckaya and Ivanova, 1956, including the subovate outline of the valve, a narrow ridge or a faint swelling linking the anterodorsal node to the mediodorsal margin, and the development of short spines on the cardinal corners (Williams et al., 1994; Vannier et al., 2005). However, a definite assignment to the family Cambriidae is precluded due to the absence of an anterodorsal cusp (*sensu* Hou et al., 2001) or an anterior cardinal corner passing into a more or less abrupt anterior-dorsal downslope which terminates at the anterodorsal corner (*sensu* Hinz-Schallreuter et al., 2007). The faint unevenness of the hinge line observed in some lateral views is either due to breakage (Figs. 7.2, 8.8), compression (Fig.7.1), or to the projection of the anterodorsal ridge beyond the dorsal margin (Fig. 7.11, 7.13). The presence of faint straight hinge lines have already been reported in the Cambriid Family (Hou et al., 2001; Hinz-Schallreuter et al., 2007), but only in specimens preserved as open valves, which necessarily involves post-mortem compression resulting in the removal of the cusps (see e.g. Petrianna Siveter et al, 1996: fig. 6j; *Cambria danvizcainia* Vannier et al., 2005, fig. 4b). Considering the very small size of the study specimens compared to described adults (6 mm to 17.5 mm according to Hou et al., 2001), it is also likely that the Pyrenean specimens represent early growth stages which have not yet developed the diagnostic features of the family. Although the Cambriidae typically show postplete to subamplete valves (with maximum height reached at or slightly behind mid-length

of the valve; Siveter et al., 1996; Hou et al., 2001; Williams et al., 2006), some studies have demonstrated the presence of preplete valves during the early development of many lineages (Zhang, 2007). However, the ontogeny of the Cambriidae and their morphological variations are poorly known (Williams et al., 1994), and only highly disputable hypotheses can be made by analogy with the closest families. For instance, the appearance of the dorsal cusp in the Kunmingellidae is generally mentioned in pre-adult stages (instar 4 of Zhang, 2007), at the same time as the lobation. If one considers a similar pattern among the Cambriidae, a dorsal-cusp should be also present in our specimens, which exhibit distinct lobation.

Although Zhang (2007) and Williams et al. (2006) consider the anterodorsal cusp as a diagnostic feature for the Kunmingellidae, it is weakly developed and commonly indistinct. Due to the lack of distinct connecting ridges, some specimens described herein (although small and poorly preserved) may, at a first glance, share more features with the Kunmingellidae than with the Cambriidae. However, the corresponding valves (Fig. 9) are among the smallest of the studied assemblage. This is again consistent with the interpretation of the entire assemblage as illustrating different growth stages of a single taxon. If right, this interpretation further suggests that the nodes appear earlier than the ridges and the cardinal spines in the ontogeny of Cambriidae.

A straight and well-developed hinge line is present in the Family Hipponicharionidae, which can also show a ventral connection between the anterior and posterior lobes (Hou et al., 2001; Williams et al., 2006; Zhang, 2007). However, the subtriangular amplete shape of the valves, diagnostic for the family, is already well developed in their earliest growth stages (Zhang, 2007), which is not the case in our material. The lobes and ridge described herein further differ from the broad, lobe-like connection between the anterior and posterior, less differentiated lobes typical of the Hipponicharionidae.

Even though a granulose, pustulose and reticulate ornamentation sporadically occur in most bradoriid families (Hou et al., 2001; Vannier et al., 2005; Williams et al., 2006; Zhang et al., 2007), the ornament of broadly spaced hollow spines has been described only in a few taxa (Skovsted et al., 2006; Topper et al., 2007). Relevant similarities can be pointed out with the ornamentation of *Spinospitella* Skovsted, Brock and Paterson, 2006 (Skovsted et al., 2006: fig.6-9; Topper et al., 2007: fig.9), although the overall description of the valve strongly differs from our observations. Notable differences include the presence, in the specimens described by Skovsted et al. (2006: figs.7i, 8d), of several spines sharing the same base and smaller spines covering the surface of the larger ones, in a crown-like arrangement. The average length of spines in our specimens is slightly lower than the measurements of Topper et al. (2007), who mention their smaller size and more rounded shapes in juveniles. Furthermore, the spinose ornamentation seems to develop in preferential parts of *Spinospitella* according to its ontogeny (Skovsted et al., 2006). A similar tendency is observed herein, with the smallest specimens lacking any distinct ornamentation and the largest specimens being entirely spinose, while the intermediate ones exhibit a pustulose ornamentation restricted to the external side of nodes.

Phylum MOLLUSCA Cuvier, 1797

Class uncertain

Order PELLAGIELLIDA Mackinnon, 1985

Family PELLAGEILLIDAE Knight, 1956

Genus *Pelagiella* Matthew, 1895

Type species.— Cyrtolites atlantoides Matthew, 1894; Cambrian Stage 3?, New Brunswick, Canada.

Diagnosis.— See Kouchinsky et al. (2011).

Pelagiella sp.

Fig. 10

Material.— More than one hundred ~~of~~ internal molds, including the figured specimens USTL XX, XX, XX.

Occurrence.— Sample TE2F.

Description.— The univalve conch is dextrally coiled with about one rapidly expanding whorl (Fig. 10.1, 10.3, 10.5, 10.7, 10.9, 10.11). The conch is asymmetrical as the spire is flat to concave on the adapical side and convex on the abapical side (Fig. 10.2, 10.4, 10.6, 10.8, 10.10). The width of the cross-section rapidly expands toward the apertural region where it reaches its maximum. There, the cross-section is suboval (Fig. 10.2, 10.4) to subtriangular with a slight angle on the abapical apertural margin (Fig. 10.8). The apex is slightly bulbous (Fig. 10.3, 10.5, 10.7, 10.9, 10.11). The external surface of the internal mold is smooth (Fig. 10.8, 10.12). The maximum diameters range from 518 μm to 1.12 mm, the aperture widths from 385 μm to 733 μm, and the shell heights from 245 μm to 467 μm.

Remarks.— The specimens described above are assigned to the genus *Pelagiella* due to their dextrally coiled conches composed of one to two rapidly expanding whorls with a flattened, slightly convex or concave spiral surface (Kouchinsky et al., 2011). The genus is subdivided into more than twenty species, sometimes highly similar in shape and bearing intraspecific variations, which emphasizes the necessity of a systematic revision (Parkhaev, 2004; Devaere et al., 2014b). Based on the lack of distinct ornamental features, any specific affiliation can only be tentative (Skovsted, 2004). The above description may correspond either to *P. madianensis*

or to *P. subangulata*, yet these species bear strongly similar characters and their differences are subtle to almost nonexistent in juveniles (Parkhaev in Gravestock et al., 2001). Their conspecificity has already been suggested (Parkhaev, 2004). The reduced rate of whorl coiling along with the absence of carena better recalls the shell of *P. madianensis* (synonymous of *P. adunca*, Bengtson et al., 1990; Parkhaev in Gravestock et al., 2001; Parhaev, 2004). However, these two characters present considerable intraspecific and ontogenetic variations (Parkhaev, 2004). Furthermore, *P. madianensis* differs from *P. subangulata* in having a concave supraperipheral surface, which has not been noticed in the recovered specimens. Based on its apertural cross-section, less extended than in *P. madianensis*, and its coplanar upper apertural margin and spiral, our specimens better resemble *P. subangulata*.

Phylum BRACHIOPODA Duméril, 1806

Subphylum LINGULIFORMEA Williams et al., 1996

Class LINGULATA Grojansky and Popov, 1985

Order LINGULIDA Waagen, 1885

Superfamily LINGULOIDEA Menke, 1828

Family EOOBOLIDAE Holmer Popov and Wrona, 1996

Genus *Eoobolus* Matthew, 1902

Type species.— *Obolus (Eoobolus) triparilis* Matthew, 1902; Wuliuan, Cape Breton, Canada.

Diagnosis.— See Balthasar (2009).

Eoobolus sp.

Figs.11-13

Material.— More than one hundred hundreds of articulated and disarticulated valves, including the figured specimens USTL XX, XX, XX.

Occurrence.— Samples TE2F, TE1E, TE1D.

Description.— The shells are inequivalved, slightly ventribiconvex (Figs. 11.1-2, 13.17) or more rarely slightly dorsibiconvex (Fig. 11.3), with its maximum width anterior to mid-length. The dorsal valves are subovate to subtriangular in outline (Figs. 12. 2-3, 12.7, 12.12, 13.1, 13. 3), and the ventral valves have an acuminate apex conferring a teardrop shape (Figs. 11.11, 11.13, 12.10, 12.15, 13.16). The pseudointerareas of both valves are subtriangular, moderately elevated above the shell floor and bear longitudinal folds or growth lines (Figs. 11.5-7, 11.10-14, 12.1, 12.4, 12.6-8, 12.11, 12.16, 12.18, 13.7-8). Ventral valves display strong flexure lines delimiting a narrow, deep median groove slightly widening anteriorly (Figs. 11.9-11, 12.10-11, 13.6-7). The partial preservation of the pseudointerarea shortens the extension of the pedicle groove which can be almost indistinguishable, but it may be expressed as a U-shaped emarginature on ventral valves (Figs. 11.9-14, 12.17-18, 13.7). On dorsal valves, the groove is shallow and broad, sometimes indistinct, and the flexure lines are weak to almost absent (Figs. 11.4-7, 12.1-8). Immediately in front of the pseudointerarea lies a visceral platform that may be extended anteriorly to about one third of the valve into a median axis. In ventral valves, the visceral platform and its proximal projection are rarely preserved, but can be inferred from scars of pedicle nerves (Fig. 11.14-15) or umbonal muscles (first central muscles according to Balthasar, 2009; Fig. 12.11, 12.18). In dorsal valves, the visceral area is divided into a proximal

and a distal portion, yet the latter is rarely preserved or tends to disappear proximally (Fig. 11.4). It may be bisected by a median depression or ridge (Fig. 12.1-3).

Subovate muscle scars may be present on the posterior portion of the dorsal visceral platform, immediately beyond the flexure lines of the pseudointerarea (first lateral muscles, Fig. 11.7), or beyond the median groove (first central muscles, Fig. 12.8, 12.18). Larger subcircular muscle scars may also occur at both sides of the median projection of the visceral platform (second central muscle scars, Fig. 11.6, 11.8, 12.5-6). One specimen shows subovate, slightly diverging muscle scars in the anterior portion of the visceral platform (third central muscles, Fig. 12.12-13). Some characters in *Vascula lateralia* are weak, arcuate to straight and begin from the proximal end of the pseudointerarea to about mid-length of the valve, following its margins (Fig. 12.1, 12.10, 12.16, 12.18). A radiating network of fine depressions is present in the internal surface of some valves, and tends to be more prominent on their peripheral parts (Fig. 13.1-5). Both valves may also show growth lines paralleling the valve margin on their anteriormost parts (Fig. 12.3, 12.17). Polygonal structures may be present on the posterior half of well-preserved valves (Fig. 11.15). They tend to be best developed in dorsal valves at the junction between the second central muscle scars and the proximal margins of the posterior part of the visceral platform (Fig. 11.6, 11.8), but they can also occur between the pseudointerarea and the valve floor (Fig. 13.8). The shell microstructure consists of fine laminae separated by a dense network of transverse columns (Fig. 13.10).

The outer surface of juvenile valves shows a subcircular, strongly convex larval shell on which a lobation is tentatively inferred from weak sublinear depressions (Fig. 13.16-18). This structure is ornamented with a dense network of tiny pits, ~ 0,7–1,5μm in diameter (Fig. 13.20). The post-larval shell of juvenile specimens is covered with fine, closely spaced pustules, around 7-10 μm in diameter (Fig. 13.19). Adult shells are depleted of any ornamental feature and only bear fine growth lines parallel to the valve margin (Fig. 13.15). A larval shell is

suggested by a rounded convex area located on the posterior end of the valve, but lacks the pitted ornament observed on juvenile specimens (Figs. 12.9, 13.11-12). This area seems to consist of at least two lobes located on its proximal margin. Adult shells may also bear a shallow, broad sulcus better developed proximally (Fig. 13.13-14). Measurements are provided in Table 1.

Remarks.— The pustulose and pitted ornament covering the adult and larval shells, respectively (Fig. 13.19-20), is a diagnostic feature of the family Eoobolidae (Holmer et al., 1996). Balthasar (2009) suggested the abolition of the Family Eoobolidae and reassigned *Eoobolus* to the Family Zhanatellidae, pointing out the importance of preservational biases on the diagnostic features of the Eoobolidae. However, Zhang et al. (2015) noticed that most specimens of *Eoobolus* lack the apical emarginature on ventral valves characterizing the Zhanatellidae. As a consequence, our specimens share the diagnostic characters of the Family Eoobolidae despite the lack of ornamental features on adult shells and the presence of an emarginature on most ventral valves. The specimens described above are assigned to the genus *Eoobolus* because of the elevated position of the pseudointerarea and its flexure lines, the deep and narrow pedicle groove on the ventral valve, the presence of a median projection of the visceral platform commonly bisected by a median ridge (in some cases abraded into a median depression in our specimens) and the shape and position of muscle scars (Balthasar, 2009). Notable differences with the genus *Eoobolus* include: (1) the presence of a fine network of radiating ridges on the inner side of some valves (Fig. 13.1-5); and (2) the diverging morphology of the third central muscle scars in one dorsal valve (Fig. 12.12-13). The latter differs from the specimens of Balthasar (2009) on which exceptionally well-preserved dorsal valves show subparallel, closely spaced muscle scars separated by a prominent median ridge. Moreover, in contrast to *Eoobolus*, the Pyrenean specimens have a very slightly elevated pseudointerarea.

Any assignment at the specific level relies on the apical angle of the ventral valve, which seems to represent the only constant feature during ontogeny (Balthasar, 2009). The ventral valves described above show apical angles ranging from 50 to 140°, preservational biases accounting for extreme values. Out of the total of 50 ventral valves, almost half of them show apical angles ranging from 80 to 90°. This short range has already been reported for *E.* aff. *viridis* from South China (Li and Holmer, 2004; Balthasar, 2009). However, angles between 70 and 80° are also common (8 valves) which can also support an assignment to both *E. elatus* and *E. priscus,* for which apical angles range from 70 to 90° (Balthasar, 2009). Finally, apical angles below 70° are also reported for 7 valves, which may indicate the presence of *E. triparilis* among the previously listed species.

The specimens described above are different from all known species of *Eoobolus* in being ventribiconvex, having subequal length and width and a short pseudointerarea, especially in dorsal valves (Table 1). The smallest L/W ratio fits with *E.* aff. *viridis* from Australia (1.15 on average; Ushatinskaya and Holmer in Gravestock et al., 2001), yet the average apical angle is much more gentle (100–110°). Valves of *E.* aff. *viridis* from China are not entirely preserved, which precludes any dimensional comparison (Li and Holmer, 2004). Dorsal pseudointerareas of *E.* cf. *triparilis* from Canada occupy 14% of the valve length and 50% of the valve width (Balthasar, 2009), which is identical to our averaged measurements (Table 1). However, the pseudointerareas on ventral valves are far more extended and bear a strongly acute apical angle. The valves described above are more similar to *E.* aff. *viridis* from China in having an apical angle of mostly 80–90°, a short pseudointerarea (compared to specimens from Australia), a diverging median groove, weak to indistinct flexure lines on dorsal valves, and a median sulcus (Li and Holmer, 2004). The pustulose ornamentation of the Chinese material, large and coarsely distributed, is also a distinctive feature shared with the specimens from the Terrades inlier. The valves described above differ from Chinese specimens in having a less elevated median ridge,

yet this feature probably derives from abrasion. The shallow, poorly defined radiating ridges observed here are also seen on specimens from South Australia, referred to *E. priscus* (Paterson et al., 2007, fig. 3C), but their sporadic occurrence questions their taxonomic significance. Polyspecificity is not excluded given the high variability of the studied specimens, for instance shown by their broad range of apical angle values.

Polygonal patterns (Figs. 11.8, 11.15, 13.7) have already been reported for a number of tommotiid (e.g. Devaere et al., 2014) and brachiopod taxa including *Eoobolus* (Balthasar, 2009). These structures are interpreted to be the precursors of organic sheaths of calcite fibers, typically known from shells built by fibrous calcite (Holmer et al., 2009).

Phylum uncertain

Class HYOLITHA Marek, 1963

Order HYOLITHIDA Sysoev, 1957

Family uncertain

Genus *Microcornus* Mambetov, 1972

Type species.— *Microcornus parvulus* Mambetov, 1972, Cambrian Age 3, Kazakhstan.

Diagnosis.— See Kouchinsky et al., 2015.

Microcornus cf. *petilus*

Fig. 14

Material.— Several tens of internal molds, including the figured specimens USTL XX, XX, XX.

Occurrence.— Sample TE2F.

Description.— Broadly orthoconic conch, 1 to 1.25 mm in length, with straight lateral margins and small apical angle (Fig. 14.1, 14.4, 14.6-7). The ventral side is flattened to weakly convex, and the lateral sides rounded, forming two longitudinal ridges (Fig. 14.2-3). The dorsal side is strongly convex bearing a weak median longitudinal ridge, producing a triangular cross-section with rounded edges (Fig. 14.2). The protoconch is bulbous, tapering into a nearly straight, rounded tip (Fig. 14.1, 14.4-7). It is separated from the mature conch by a shallow constriction (Fig. 14.1, 14.4-5). The surface of the internal mold exhibits a weak polygonal network located on the bulbous protoconch, and gradually disappearing after the constriction (Fig. 14.4-7). Neither opercula nor ligula are observed. The apertural width and height range from 350 µm to 435 µm and from 170 µm to 215 µm, respectively. The apical angle is about 15 °.

Remarks.— The specimens described above are assigned to the genus *Microcornus* based on their overall shape with a bulbous protoconch, a median ridge on the dorsal side and the resulting rounded triangular cross-section (Bengtson in Bengtson et al., 1990; Malinky and Skovsted, 2004). The narrow conical morphology of the conchs produced by a small apical angle, along with the weakly convex ventral side conforms to *Microcornus petilus* Bengtson, 1990 (Bengtson in Bengtson et al., 1990; Demidenko in Gravestock et al., 2001; Malinky et al., 2004; Topper et al., 2009). However, the specimens exhibit a notable difference with *M. petilus*: the polygonal network located on the bulbous protoconch. Such a pattern has never been mentioned on internal molds of hyolithids, and probably reflects the ornamentation of the inner surface of the conch.

Order uncertain

Family CUPITHECIDAE Duan, 1984

Genus *Cupitheca* Duan in Xin et al., 1984

Type species.— *Paragloborilus mirus* (He in Qian, 1977), Fortunian, Maidiping, Emei County, Sichuan Province, South China.

Diagnosis.— See Parkhaev and Demidenko (2010).

Cupitheca sp.

Fig. 15

Material.— 10 specimens, including the three internal molds USTL XX, XX and XX and two coatings USTL XX and XX.

Occurrence.— Sample TE2F.

Description.— The conchs are slowly and uniformly expanding throughout their length (Fig. 15.1, 15.3). The maximum length ranges from 426 μm to 1.15 mm, the maximum abapical diameter of the conch from 224 to 813 μm, and the diameter of rods from 2.5 to 6 μm. They are always abapically broken so only a short, straight part, including the closed termination, is preserved. The cross section is subcircular to oval. The closed termination (apex) is slightly (Fig. 15.1) to strongly (Fig. 15.7) convex and a shallow but well-defined constriction separates

it from the conch (Fig. 15.1-3, 15.7-9). At the apex, internal and external coatings of the conch wall are connected with transverse phosphatic rods expressed as tiny pits on the surface of the external coating (Fig. 15.4, 15.9-11). The external coating exhibits faint transverse striations (Fig. 15.3, 15.5).

Remarks.— The recovered conchs are assigned to the genus *Cupitheca* based on their gently tapering conical shape with a convex apex separated by a marked constriction. Their identification at the specific level remains open as the ornamentations of faint transverse striations are not typical of any species of *Cupitheca*. The evidence of faint annular sculptures on the external surface together with the presence of a rod-like microstructure is comparable to one specimen of *C. holocyclata* described by Malinky and Skovsted (2004, fig. 12A).

Phylum, class uncertain

Order TOMMOTIIDA Missarzhevsky, 1970

Family uncertain

Genus *Kelanella* Missarzhevsky *in* Rozanov and Missarzhevsky, 1966

Type species.— *Kelanella altaica* Missarzhevsky in Rozanov and Missarzhevsky, 1966, Cambrian Age 5, Altai Mountains, Siberian Platform, Russia.

Diagnosis.—See Devaere et al. (2014b)

Kelanella altaica Missarzhevsky in Rozanov and Missarzhevsky, 1966

Figs. 16-19

Material.— About 80 specimens, mostly fragmentary; 20 sclerites identified to belong to type A (5), type B (1), type C (9) and type E (5).

Occurrence.— Samples TE2F, TE1D and TE1E.

Description.— Following the nomenclature of Devaere et al. (2014b), four morphological types were identified herein. Type A sclerites (Fig. 16) are bilaterally symmetric to subsymmetric, the apex slightly bending over the duplicature (Fig. 16.1-2). The cross-section is crescent-shaped (Fig. 16.7, 16.10). The broad convex facet shows a gridded ornament which consists of a radiating network of irregularly-spaced longitudinal folds and more discrete transversal ribs (Fig. 16.3-4, 16.8, 16.12). This ornamentation is well-developed in the apertural region and gradually disappears toward the apex (Fig. 16.3). The opposite, concave duplicature shows fine subparallel transverse growth lines slightly curving to the apical region following the shape of the apertural margin (Fig. 16.5-6, 16.11). They seem to be continuous with the transverse ridges of the gridded facet (Fig. 16.11). Reduced lateral facets are present between the gridded facet and the duplicature (Fig. 16.5).

Type B sclerite (Fig. 17) is asymmetrical, polyhedron-shaped and wider than type A (Fig. 17.3, 17.5). The centrally-situated apical area (apex not preserved) gently curves over the duplicature (Fig. 17.1-2). The weakly convex gridded facet displays a subparallel, closely-spaced network of transverse ridges overlapping irregularly-spaced longitudinal folds radiating from the apical region (Fig. 17.3-4). The asymmetry of the specimen is based on a deep sulcus situated on the convex gridded facet, extending from the apical region to the aperture, where it is expressed as a notch (Fig. 17.2-3). The slightly convex duplicature bears fine subparallel growth lines that are prolonged into more elevated ridges in two lateral facets (Fig. 17.5-7). A suboval cross-section is visible in the apical region due to breakage (Fig. 17.5-6).

Type C sclerites (Fig. 18) are slightly asymmetrical (Fig. 18.4-5) with a subrectangular cross-section (Fig. 18.2, 18.6-7, 18.11). The apertural region is more or less strongly curved over the duplicature (Fig. 18.1-2, 18.6, 18.11, 18.14). The gridded facet is concave to weakly convex (Fig. 18.2, 18.6). The opposite duplicature runs from concave toward the aperture to planar in the apical region (Fig. 18.6-7, 18.11). It may bear a fine network of subparallel growth lines, gradually curving toward the apical region (Fig. 18.4, 18.10). The gridded facet and the duplicature are separated by two concave-to-planar lateral facets (Fig. 18.1, 18.3, 18.11, 18.14). The ornamentation of the gridded facet consists of well-defined, broad longitudinal folds that tend to disappear toward the apical region (Fig. 18.1-2, 18.12). These irregularly-spaced radiating lines are overlapped by weaker transverse ridges in a gridded arrangement. In some specimens, the lateral facets bear a transitional ornamentation consisting of discrete to absent longitudinal folds and well-defined transverse ridges gradually attenuating toward the duplicature margin (Fig. 18.3, 18.11, 18.14). Our largest specimen shows, nonetheless, a strong gridded ornamentation on its lateral facets (Fig. 18.1-2). Transverse internal septa are observed in broken specimens (Fig. 18.6, 18.9-10, 18.15).

Type E sclerites are asymmetrical, slightly twisted (Fig. 19.1-2). The apical area is strongly curved toward the duplicature (Fig. 19.2-3). The gridded facet is partially separated from the opposite concave duplicature by a single, subplanar to concave lateral facet (Fig. 19.1-2, 19.4). The transition between the lateral facet and the duplicature may be marked by a weak longitudinal crest (Fig. 19.2). The ornamentation on the gridded facet consists of broad longitudinal folds radiating from the apex, superimposed by thinner transverse ridges (Fig. 19.3). The lateral facet only bears well-developed transverse ribs (Fig. 19. 1-2, 19.4).

In one broken specimen that cannot be assigned to any type, the internal cavity shows slightly concave transverse septa, one of which possesses a polygonal network of fine ridges (Fig. 19.5-6).

Measurements have been done following Devaere et al.'s (2014b) stated dimensions. The maximum height ranges from 1.2 to 1.9 mm for type A, 1.6 mm for type B, 1.2 mm to 2.1 mm for type C, and 870 μm to 2.1 mm for type E. The length ranges from 93 to 225 μm for type A, unavailable for type B, 555 to 875 μm for type C, and 93 to 300 μm for type E. The maximum width ranges from 600 μm to 1 mm for type A, 2.4 mm for type B, 2.7 mm for type C, 475 μm to 1 mm for type E.

Remarks.— The sclerites described above are assigned to the genus *Kelanella* on the basis of their overall polyhedral shape, the presence of transverse septa and facets, one of which bears a gridded ornament. The single specimen assigned to type B shows a noticeable difference with the specimens described by Devaere et al. (2014b) in the presence of fine, discrete and closely-spaced growth lines on the duplicature (Fig. 17.5-7), along with prominent and elevated folds on the gridded facet (Fig. 17.3-4). Although the affiliation of this peculiar type to *Kelanella altaica* has been questioned by Devaere et al. (2014b), the recovery of the type B sclerites together with other sclerites undoubtedly assigned to *Kelanella altaica* supports the assumption that they belong to the same scleritome. One specimen assigned to type C, due to its quadrangular cross-section, shows a strong gridded pattern on its lateral facets (Fig. 18.1-2) which has never been described in this type. Polygonal structures have already been described for type E sclerites (Devaere et al., 2014b), other tommotiids (e.g. *Eccenthroteca*) and brachiopods (e.g. *Eoobolus*). They are interpreted as remains of organic layers indicating that tommotiids and brachiopods shared the same mode of skeletal secretion, which further support their phylogenetic relationship.

Order CHANCELLORIIDA Walcott, 1920

Family CHANCELLORIIDAE Walcott, 1920

Remarks.— The taxonomy of chancelloriids in this study is based on disarticulated sclerites which are the only available material. The taxonomy and terminology follow Moore et al. (2014).

Genus *Chancelloria* Walcott, 1920

Type species.— *Chancelloria eros* Walcott, 1920, Cambrian Age 5, Walcott Quarry, Ontario, Canada.

Diagnosis.— See Kouchinsky et al. (2011).

Chancelloria sp.

Fig. 20.1-6.

Material.— A dozen of slightly broken to complete internal molds of sclerites including the figured specimens USTL XX, XX, XX.

Occurrence.— Sample TE2F.

Description.— The 7+1 sclerites consist of radiating lateral rays surrounding a larger, subvertical central ray in a star-like appearance (Fig. 20.1-2, 20.4-5). Lateral rays are mostly regularly oriented, straight and parallel to the basal surface at least for their most proximal part (tips are not preserved). Rays are separated from one another by deep narrow grooves. A verruculose texture produced by small, densely distributed bumps is visible on the external surface of some rays, tending to be better developed proximally (Fig. 20.3). Scale-like

structures visible on the external surface of some rays may locally results in a fibrous appearance (Fig. 20. 6). The maximum length of ray is 1.03 mm (all fragmentary). The angle between rays varies from 40 to 75° for irregular sclerites, but is ~ 60° for regular ones. The diameter of central ray ranges from 352 μm to 755 μm.

Remarks.— The specimens described above are assigned to *Chancelloria* because of their flattened basal surface consisting of 7 regularly oriented lateral rays distributed over one plane, surrounding a larger, subvertical central ray (Fig. 20.1-2, 20.4). Specimens from the Terrades inlier are comparable to *Chancelloriella irregularis*, for which 7+1 sclerites are common (Moore et al., 2014). However, the irregularity in orientation and shape of its lateral rays contrasts with the sclerites described above. Small cylindrical to conical bumps (Fig. 20.3) have already been reported among the Chancelloriidae, and interpreted to represent infills of pores initially piercing the calcareous wall of the sclerite dissolved by acid treatment (Moore et al., 2014). Scale-like textures of internal molds (Fig. 20.6) are known from several chancelloriid genera, and are interpreted to represent inclined projections of an underlying layer of aragonitic fibers (Porter, 2008; Moore et al., 2014).

Genus *Allonnia* Doré and Reid, 1965

Type species.— *Allonnia tripodophora* Doré and Reid, 1965, Cambrian Age 2?, Carteret, Armorican Massif, France.

Diagnosis.— See Moore et al. (2014).

Allonnia tetrathallis (Jiang, in Luo et al., 1982)

Fig. 20.7-14.

Material.— A dozen of slightly broken to complete internal molds of sclerites including the figured specimens USTL XX, XX, XX.

Occurrence.— Sample TE2F.

Description.— The 4+0, 5+0 and 6+0 sclerites exhibit lateral rays that steeply bent away from the basal surface; no central ray is observed. The maximum width of the rays is reached on its proximal end, tapering distally into a pointed tip (Fig. 20.8-9, 20.11-12). Deep and narrow grooves separate each lateral ray. In 4+0 sclerites, two rays bear three articulatory facets and therefore touch three other rays, whereas two rays bear two articulatory facets and are in contact with only two other rays (Fig. 20.7-8). Rays bearing three articulatory facets are slightly longer than the others. The rays contact nearly at right angles to each other in abaxial view. 5+0 sclerites have one larger ray in contact with the 4 others, two rays in contact with three other rays, and two rays in contact with two other rays (Fig. 20.9-10). 6+0 type sclerites are represented by two specimens with variable arrangement of the lateral rays (Fig. 20.11-14). The length of rays ranges from 380 to 725 μm, the angles between rays are 70° on average for 6+0 type sclerites and 90° for 4+0 type sclerites. The angle between lateral rays and the basal surface ranges from 25 to 55° for 6+0 and 4+0 sclerite types, and is around 30° for the 5+0 sclerite type.

Remarks.— The sclerites described above are assigned to the genus *Allonnia* because of the absence of central rays and the strongly angled position of lateral rays from the basal plane, pointing out from the flattened basal surface. Within the genus, the Pyrenean sclerites are assigned to *A. tetrathallis* due to the similarities between the 4+0 and 5+0 forms already assigned to the species in the literature (see Moore et al., 2014). 6+0 forms found in the Cambrian Puerto Blanco Formation of NW Mexico were tentatively assigned to *A. tetrathallis*

(Devaere et al., in press). 6+0 forms with the general morphology of *A. tetrathallis* have also been recovered from the Terrades inlier and support the assignment of this form to the species.

Genus *Archiasterella* Sdzuy, 1969

Type species.— *Archiasterella pentactina* Sdzuy, 1969.

Diagnosis.— See Moore et al. (2014).

Archiasterella charma Moore, Li and Porter, 2014

Fig. 20.15-17

Material.— Two internal molds of sclerites including the figured specimens USTL XX.

Occurrence.— Sample TE2F.

Description.— The 3+0 sclerites without central ray, consist of two horizontal rays oriented parallel to the basal surface and one principal ray recurved over the two others (Fig. 20.15-16). In its proximal region, the principal ray is larger than the two lateral rays (Fig. 20.16) but its basal facet is smaller (Fig. 20.15). The cross-section of each ray is subcircular distally and oval proximally. It is pierced on its basal facet by a central, subcircular to oval foramen which is smaller in the principal ray (Fig. 20.15). A Y-shaped deep narrow groove is situated close to the foramina, separating each ray. A verruculose texture is visible on the external surface of the rays, but it is better expressed distally (Fig. 20.16-17). The principal ray curves at ~45° above the basal surface. The angle between lateral rays is ~145°. All rays are fragmented, with a

maximum length of 515 μm. The major axis of foramina is ~156 μm for lateral rays and 93 μm for the principal ray. The minor axis is ~99 μm for lateral rays and ~55 μm for the principal ray.

Remarks.— The specimens described above are assigned to the genus *Archiasterella* based on the absence of central rays and the coplanar position of the two lateral rays, with the principal ray recurved over the latter (Moore et al., 2014). In this genus, three-rayed sclerites have only been reported in the species *Archiastrella charma*.

Order HYOLITHELMINTHIDA Fisher, 1962

Remarks.— Due to the uncertain systematic position and paleobiology of hyolithelminth tubes, along with their conspicuously simple shape showing considerable variations, new genera and species within the order have proliferated. The discrimination between taxa relies on subtle differences related to the general shape, the outline of the cross-section, the angle of divergence and the morphology, and the density and prominence of the ornamentation. Numerous studies have shown the high variability of these characters among single taxa and their probable relationship with preservational biases (e.g., see Skovsted et al., 2006). Moreover, distinctions at the generic level have been questioned by the discovery of transitional forms (Paterson et al., 2007; Topper et al., 2009). Nonetheless, for reasons of clarity, the traditional taxonomy will be used with open nomenclature for the following systematic analyses.

Family HYOLITHELLIDAE Walcott, 1886

Genus *Hyolithellus* Billings, 1871

Type species.— *Hyolithes micans* (Billings, 1871), Cambrian Age 4, Troy, New York State, USA.

Hyolithellus sp.

Fig. 21.1-9

Material.— About 50 fragmented phosphatic tubes, including the figured specimens USTL XX, XX, XX.

Occurrence.— Samples TE2F, TE1E and TE1D.

Description.— The subcylindrical tubes of phosphatic composition have a subcircular cross-section at both opened ends (Fig. 21.2-4, 21.7-8). All specimens are fragmentary. They are generally slightly tapering toward one end, straight (Fig. 21.4-5, 21.9) to curved (Fig. 21.1). The external surface of the tube is either smooth (Fig. 21.4) or with regularly-spaced, faint (Fig. 21.6) or irregular, dense, transverse annulations that can be interrupted at mid-length (Fig. 21.5, 21.9). The length ranges from 571 μm to 1.7 mm, the maximum diameter of the cross-section from 136 μm to 670 μm, and the angle of divergence from 1 to 8°. The spaces between ribs range from 20 to 80 μm.

Remarks.— The specimens described above are assigned to the genus *Hyolithellus* based on their phosphatic composition, their slightly tapering cylindrical shape and their circular cross-section. Nearly straight tubes covered with weak and regularly spaced annulations are comparable to *H. micans* Billings, 1871, whereas the tubes with more irregular and coarser ornamentation (Fig. 21.3-4) are similar to *H. filiformis* Bengtson in Bengtson et al., 1990, although the available material is too fragmentary to preserve their complete curved shape (Demidenko in Gravestock et al., 2001; Topper et al., 2009).

Family TORELLELLIDAE Holm, 1893

Genus *Torellella*? Holm, 1893

Type species.— *Hyolithes laevigatus* (Linnarson, 1971), Cambrian Age 3, Sweden.

Remark.— Phosphatic tubes with an elliptical cross-section, a planar apertural margin and transverse annulations are generally referred to *Torellella* (Skovsted et al., 2006). However, this genus shares an important set of features with *Sphenothallus* and their distinction relies on highly subtle details, which may be strongly controlled by preservational biases (Yang et al., 2014). They include ornamental features (Zhu et al., 2000), yet this criterion is delicate to take into account given the scarcity of well-preserved microstructures on the material described above. Another distinctive feature concerns longitudinal thickenings located on the narrow sides of the tube (in transversal view). Due to the difficulties for identifying these characters, the present material is only tentatively assigned to *Torellella*.

Torellella? sp.

Fig. 21. 10-28

Material.— About a hundred phosphatic tubes, more or less fragmented, including the figured specimens USTL XX, XX, XX.

Distribution.— Samples TE2F, TE1E and TE1D.

Description.— The straight (Fig. 21.20), curved (Fig. 21.14-15, 21.25) or slightly undulating (Fig. 21.10, 21.19, 21.26) phosphatic tubes have an elliptical cross-section (Fig. 21.11, 21.13-14, 21.18-19, 21.22-23). The latter becomes circular adapically as the tube tapers (Fig. 21.12, 21.17). The angle of divergence (from 6 to 23°) generally increases toward the aperture (Fig. 21. 15, 21.26). The apical end may bear an expanded margin separated by the rest of the tube by a low constriction (Fig. 21.15). In the apertural region, the broad sides are flat (Fig. 21.14, 21.19) to slightly convex (Fig. 21.13, 21.22). The external surface of the tubes is generally smooth but, when preserved, the external ornament consists of faint transverse ribs (Fig. 21.27-28), separated by a distance of about 20 µm. Narrow sides are rounded and may exhibit fine, discrete longitudinal ridges (Fig. 21.24-25). All specimens are fragmented, from 938 µm to 3 mm in length, and 140 µm to 813 µm in maximum diameter.

Remarks.— The conical structure at the apical end may act as an attachment mechanism to the substrate, although no attachment disk was recovered.

Family uncertain

Genus *Rhombocorniculum* Walliser, 1958

Type species.— Helenia cancellata Cobbold, 1921; Cambrian Age 3, lower Cambrian; Comley, Shropshire, Britain.

Diagnosis.—See Kouchinsky et al. (2015).

Rhombocorniculum cancellatum Cobbold, 1921

Fig. 22

Material.—Five entire to partially broken sclerites, all figured herein.

Occurrence.— Sample TE2F.

Description.— The sclerites are elongate, variably curving up to ~70° and strongly twisting up to ~90° clock- (Fig. 22.3-4) or anticlockwise (Fig. 22.5). They consist of a slender type (Fig. 22.3-5) and a broad type, the latter represented by a single specimen (Fig. 22.1-2). The slender sclerites exhibit two broad sides, one convex and the other slightly concave, and two thin margins, one thicker than the other, which can be blade-like thus producing an asymmetric drop-like cross-section (Fig. 22.3-6, 22.8). The latter displays a small circular to oval opening, called lumen, and is surrounded by a thick wall (Fig. 22.3-4, 22.8). The lumen can also be a planar-convex crescent-like opening paralleling the margins of the cross-section, with a reduced wall (Fig. 22.5-6). The external surface is covered by a cancellate ornamentation, consisting of a dense network of fine, regularly-spaced tubercles (Fig. 22.1, 22.3, 22.7, 22.9). These latter, when well-preserved, seem to be perpendicular to the surface. The broad type differs from the slender one in bearing two broad lateral surfaces, one flat and the other slightly convex, thus producing a thin and elongated, almost rectangular cross-section (Fig. 22.2). In this morphotype, the lumen is small, oval in cross-section and central to the cross-section of the sclerite. The sclerites are from 1.09 mm to 1.74 mm in length (maximum distance between the apex and the aperture), from 167 µm to 424 µm in width (maximum distance between the lateral sides of the apertural cross-section), and from 47.5 µm to 120 µm in height (maximum distance between upper and lower sides of the apertural cross-section).

Remarks. —The recovered sclerites are assigned to the genus *Rhombocorniculum* on the basis of their typical cancellate ornamentation, elongated shape and the presence of a central lumen

(Kouchinsky et al., 2015). The diagnostic microstructure of obliquely-arranged tubules covering the wall is not preserved. The recovered sclerites show a twisted shape with tubercles perpendicular to their surface and a thick wall associated to a drop-shaped cross-section, which enables the assignment to *R. cancellatum*. However, one specimen clearly shows a reduced wall and a strongly developed opening (Fig. 22.5-6), which questions its affiliation to this species. The Pyrenean specimens differ from *R. insolutum* which shows either bifurcated, spine-like or very broad morphotypes.

Indeterminate subconical elements

Fig. 23

Material.— More than fifty broken internal molds, some with fragments of external coating, including the figured specimens USTL XX, XX, XX.

Occurrence.— Sample TE2F.

Description.— The subconical elements are straight (Fig. 23.19, 23.22, 23.24) to curved (Fig. 23. 1, 23.4, 23.11-14, 23.18), 329 µm to 2.16 mm in length, 128 µm to 417 µm in width, and 112 µm to 267 µm in height. The degree of curvature, when observable, gently increases toward the apex where it reaches its maximum. The apex is curved toward the arbitrarily defined posterior region. When preserved, the apical tip is sharply pointed (Fig. 23.4, 23.11-12, 23.14, 23.18) to slightly rounded (Fig. 23.19, 23.22, 23.26). The abapical area is generally irregularly broken but one specimen has an inflated abapical end (Fig. 23.1-3). The elements are laterally flattened (Fig. 23.2, 23.13, 23.17). One specimen is strongly flattened to crinkled (Fig. 23.11, 23.16). One longitudinal furrow, situated slightly posterior to the middle line of each lateral side, is variably expressed, from faint (Fig. 23.1, 23.4, 23.12) to strong (Fig. 23.11, 23.14,

23.18-19, 23.22, 23.24). When present, furrows gradually faint toward the apex. The posterior and anterior sides are strongly convex, so the cross-section of the sclerite is “8”-shaped (Fig. 23.2-3, 23.8, 23.10, 23.13, 23.16-17, 23.23, 23.27-28) with two laterally flattened lobes. The ornamentation of internal molds consists of broadly and regularly spaced pustules, 10 µm to 15 µm in diameter, arranged in rows on the anterior and posterior margins of the element (Fig. 23.5, 23.19, 23.20); narrow longitudinal striae or furrows and elongated pits aligned in the same direction (Fig. 23.7, Fig. 23.15); and rows of faint ridges (Fig. 23.25). Spines are also visible on the posterior margin of one specimen (Fig. 23.18, 23.21). Polygonal structures may also be observed on internal molds, surrounding the pustules on the lateral surface (Fig. 23.29). One specimen exhibits a subconical element attached to a crinkled unidentified structure (Fig. 23.17-18, 23.20-21).

Remarks.— The crinkled specimens support the hypothesis that the shell/carapace was initially flexible. Such a preservation is comparable to the bradoriids recovered from the same level. Moreover, the crinkled unidentified structure to which a conical element is connected broadly resembles that of the bradoriids. Finally, conical elements and bradoriids share similar ornamentations. Recently, ornamented spines comparable to the unidentified subconical elements described above have been interpreted to represent detached fragments of different panarthropod origin (Skovsted and Peel, 2001; Topper et al., 2007; Dzik, 2003; Caron et al., 2013; Li et al. 2012; Zhang et al., 2014; Kouchinsky et al., 2015).

Biostratigraphic and biogeographic implications

The microfossil assemblage described above provides new data for potential international correlation of the Terrades inlier and the eastern Pyrenees. The previously recovered archeocyathan assemblage has recently been revised and assigned to Spanish Zone VI

corresponding to the Botoman zone 1 (upper part of Cambrian Stage 3; upper Ovetian according to the regional Spanish chart; Menéndez et al., 2015). However, owing to their strong tendency to regional endemism, correlations based on archeocyaths are limited to a regional scale (Peng et al., 2012). The microfossils formally identified in this study have a wider geographic extensions and well-known stratigraphic ranges that enable us to constrain the former archeocyathan-based chronostratigraphic age. The tommotiid *Kelanella altaica* has been so far reported from the Cambrian Stage 3 of China (Yuan and Zhang 1983; Qian 1989), the Cambrian Stage 5 of Russia (Rozanov and Missarzhevsky 1966; Missarzhevsky and Grigorieva 1981) and the Cambrian stages 3–4 of Antarctica (Wrona 1989, 2004) and France (Devaere et al., 2014b). The chancelloriid *Allonnia tetrathallis* is known from the Cambrian Stages 2–3 of South China (Luo et al., 1982, 1984; Qian, 1989; Qian and Bengtson, 1989; Li and Xiao, 2004; Li et al., 2004; Steiner et al., 2004; Moore et al., 2014; Yang et al., 2015) and Mexico (Devaere et al., 2019), the Cambrian Stage 3 of Germany (Elicki, 1994) and possibly the Cambrian Stage 4 of Antarctica (Wrona, 2004). Another chancelloriid, *Archiasterella charma*, has been recovered from the Cambrian Stage 2 (possibly Cambrian Stage 3) of South China (Moore et al., 2014) and the Cambrian Stages 2–3 of Mexico (Devaere et al., 2019). The most biostratigraphically significant microfossil recovered from the Terrades inlier is *Rhombocorniculum cancellatum*, which displays a worldwide distribution in Cambrian Stage 3 successions (equivalent to the upper Atdabanian–lower Botoman of the Russian chart; Kouchinsky et al., 2015). *R. cancellatum* occurs in the *Rhombocorniculum cancellatum*–*Microcornus parvulus* Assemblage Zone of China (Qian and Zhang, 1983; Yu, 1987; Qian, 1989; Yue and Gao, 1992; Yang et al., 2015), the *Rhombocorniculum cancellatum* Zone of Kazakhstan (Missarzhevsky and Mambetov, 1981), Kyrgyzstan (Missarzhevsky and Mambetov, 1981), Mongolia (Missarzhevsky, 1973, 1977; Esakova and Zhegallo, 1996; Brasier et al., 1996), Germany (Elicki and Schneider, 1992; Elicki and Wotte, 2003; Elicki,

1994, 2005) and England (Cobbold, 1920; Wallister, 1958; Brasier, 1986; Hinz, 1987; Brasier et al., 1992b), the *Judomia* to *Erbiella* trilobite zones of the Siberian Platform (Bengtson et al., 1983; Vasilieva, 1998; Varlamov et al., 2008; Rozanov et al., 2010; Korovnikov and Novozhilova, 2012; Kouchinsky et al., 2015; Korovnikov et al., 2018), the *Callavia broeggeri* trilobite Zone of Nova Scotia (Landing et al., 1980; Landing, 1995), eastern Massachusetts (Landing et al., 1988; Brasier et al., 1992a) and Newfoundland (Bengtson, 1983; Landing et al., 1988; Brasier et al., 1992b; Brasier, 1989; Landing, 1995), the *Pararaia tatei* and *Pararaia bunyerooensis* trilobite zones of Australia (Gravestock et al., 2001) and the *Holmia kjerulfi* trilobite Zone of Sweden (Bengtson, in Brasier, 1986; Brasier, 1989). The concurrent-range of other microfossils from the Terrades inlier is also restricted to the Cambrian Age 3, as a result of which the limestones from the Terrades inlier are attributed to this age, as confirmed regionally by the archeocyathan record.

The newly reported microfossils, along with previously reported archeocyaths further enable discussing the paleobiogeographic affinities of the study area. According to recent Cambrian paleogeographic reconstructions (Álvaro et al., 2013, 2021; Pouclet et al., 2016), the Pyrenean Domain was located along the western Gondwana margin, although its exact position regarding neighboring areas remain controversial. Together with the Montagne Noire (France) and Sardinia (Italy), West Gondwana comprised a mosaic of Cambrian platforms that were prolonged laterally through the Cantabrian, West Asturian-Leonese and Central Iberian, tectonostratigraphic zones of the Iberian Massif (Fig. 1). The Cantabro-Ebroan land area, which was the Cambrian source for this Gondwana margin, would lie at present below the Cenozoic Ebro Valley (Aramburu *et al*. 2002; Romero and Schimmel, 2018). Therefore, even if Cambrian Age 3 archeocyaths have been reported from the Variscan zones of the Iberian Massif, allowing direct biostratigraphic correlation with the Terrades inlier, these zones were originally situated laterally facing the same Gondwana supercontinent. Similarly, Cambrian Age 3 archeocyathan-

microbial reef complexes punctuated rifting branches of the so-called Atlas-Ossa Morena Rift, which fringed the above-reported Iberian zones (Álvaro et al., 2013, 2014a-b; Pouclet et al., 2016). Although Epoch 2 archaeocyaths have been reported from the Ossa-Morena Zone, which show some limited generic similarities with the Terrades assemblages, Cambrian paleobiogeographic affinities of the Terrades Inlier with the Occitan Domain (Montagne Noire) and Sardinia are more significant. The archaeocyathan assemblage from the Mattopa Formation (Nebida Group) of Sardinia is the most similar to that reported from the Terrades bioconstructions (Abad, 1988; Perejón et al., 1994; Laumonier et al., 1996). However, an Occitan affinity of the Terrades inlier is also supported by the microfossil assemblage described above. The Cambrian reefal and peri-reefal limestones of Terrades show strong similarities with the Pardailhan Formation of the Montagne Noire (Fig. 4). The latter, which consists of alternations of reefal and peri-reefal limestones and green shales, with subsidiary sandstone and conglomerate interbeds (Debrenne et al. 2002), is dated as Cambrian Age 3–4 based on archaeocyaths and microfossil occurrences (Álvaro et al., 2014; Devaere et al., 2014a-b). Its fossil assemblage includes hyoliths, chancelloriids, the brachiopod *Eoobolus*, the bradoriid *Monceretia erisylvia* (a Cambridae) and the tommotiid *Kelanella altaica*. The occurrences of the latter in western Europe are restricted to the southern Montagne Noire and the Terrades inlier, which gives strong supports to their close paleobiogeographic relationships.

The Terrades inlier exposes a small piece of the pre–Variscan basement in the South Pyrenean Zone, which represents a major nappe (the Cadí Nappe) overlapping the Ebro Foreland Basin to the south. However, the tectonic relationships between the basement exposed in Terrades and that of the Axial Zone have not yet been well established and different structural interpretations have been suggested (e.g., Martínez et al., 1989, 1997; Pujadas et al., 1989; Baudin et al., 2008; Laumonier, 2015). However, no structural interpretations places the source of the Terrades inlier in a Northern Pyrenean or even Occitan, pre-Alpine position, but instead

all consider it as part or direct continuation of the Axial Pyrenean Zone. As a consequence, both fossil assemblages and lithostratigraphy of the Terrades succession support strong palaeo(bio)geographic affinities between the Montagne-Noire, the Pyrenees and Sardinia.

Conclusions

The Cambrian reefal deposits of the Terrades inlier are the only known carbonates from the eastern Pyrenees that have not recorded the Variscan metamorphic degree that has transformed into marbles any Cambrian carbonates, such as those preserved, and supposedly related, in the contemporaneous Valcebollère Formation. They delicately preserve thromboid textures, archeocyaths, and small shelly fossils. The latter, described for the first time herein, include hyoliths, hyolithelminths, chancelloriids, tommotiids, bradoriids, molluscs and brachiopods. The systematic identification of many groups remains uncertain owing to their preservation as internal molds, their juvenile age and/or the need for taxonomic revisions. Along with the regional dating provided by archeocyaths, the microfossil record includes *Rhombocorniculum cancellatum* supporting a Cambrian Age 3 (Epoch 2) for the succession. Striking similarities in lithologies and fossil faunas have been pointed out with the southern Montagne Noire, especially the Pardailhan Formation, and subsidiarily with Sardinia (Italy). These interpretations support the paleopositional closeness of these western Gondwanan units, where the Pyrenean margin would represent a lateral prolongation of the Montagne Noire.

Acknowledgements

Financial support for this work was provided by the RGF program of the French Geological Survey (Bureau de Recherches Géologiques et Minières (BRGM). JJA and SC were further supported by a project from the Spanish Ministry of Sciences and Innovation CGL2017-87631-P, and International Emerging Action "ECGO" (PICS07982) co-funded by CNRS (France) and CSIC (Spain). LD benefited from a postdoctoral research fellowship of the Alexander von Humboldt Foundation.

References

Abad, A., 1988, El Cámbrico inferior de Terrades (Gerona). Estratigrafía, facies y paleontología: Batallería, v. 2, p. 47–56.

Aguilar, C., Montserrat, L., Castiñeiras, P., and Navidad, M., 2014, Late Variscan metamorphic and magmatic evolution in the eastern Pyrenees revealed by U–Pb age zircon dating: Journal of the Geological Society, London , v. 171, p. 181–192.

Álvaro, J.J., Bauluz, B., Clausen, S., Devaere, L., Gil Imaz, A., Monceret, E., and Vizcaïno, D., 2014a, Stratigraphic review of the Cambrian–Lower Ordovician volcanosedimentary complexes from the northern Montagne Noire, France: Stratigraphy, v.11, p. 83–96.

Álvaro, J.J., Bellido, F., Gasquet, D., Pereira, M.F., Quesada, C., and Sánchez-García, T., 2014b, Diachronism in the late Neoproterozoic–Cambrian arc-rift transition of North Gondwana: a comparison of Morocco and the Iberian Ossa-Morena: Journal of African Earth Sciences, v. 98, 113–132.

Álvaro, J.J., Monceret, E., Monceret, S., Verraes, G., and Vizcaïno, D., 2010, Stratigraphic record and palaeogeographic context of the Cambrian Epoch 2 subtropical carbonate platforms and their basinal counterparts in SW Europe, West Gondwana: Bulletin of Geosciences, v. 85, p. 573–584.

Álvaro, J.J., Zamora, S., Clausen, S., Vizcaïno, D., and Smith, A.B., 2013, The role of abiotic factors in the Cambrian substrate revolution: a review from the benthic community replacements of West Gondwana: Earth-Science Reviews, v. 118, p. 69–82.

Álvaro, J.J., Casas, J.M., and Quesada, C. 2021. Reconstructing the pre–Variscan puzzle of Cambro–Ordovician basement rocks in the southwestern European margin of Gondwana. In: Pannotia to Pangaea: Neoproterozoic and Paleozoic Orogenic Cycles in the Circum-Atlantic Region (Murphy, J.B., Strachan, R.A., and Quesada, C., eds.). Geological Society, London, Special Publications 503, 531–562.

Aramburu, C., Méndez-Bedia, I., Arbizu, M. & García-López, S. 2004. Zona Cantábrica. Estratigrafía. La secuencia preorogénica. In: Geología de España (Vera, J., ed.). Sociedad Geológica de España & Instituto Geológico y Minero de España, Madrid, pp. 27–34.

Babcock, L.E., Peng, S., Zhu, M., Xiao, S., and Ahlberg, P., 2014. Proposed reassessment of the Cambrian GSSP: Journal of African Earth Sciences, v. 98, p. 3–10.

Ballèvre, M., Bosse, V., Ducassou, C., Pitra, P., 2009. Palaeozoic history of the Armorican Massif: Models for the tectonic evolution of the suture zones: Compte Rendus Geosciences, v. 341, p. 174–201.

Balthasar, U., 2009, The brachiopod *Eoobolus* from the Early Cambrian Mural Formation (Canadian Rocky Mountains): Paläontologische Zeitschrift, v. 83, p. 407–418.

Baudin, T., Autran, A., Guitard, G., and Laumonier, B., 2008, Carte géologique de la France, Feuille d'Arles-sur-Tech (1100): Bureau de Recherches Géologiques et Minières, Orléans, France, scale 1/50000, 1 sheet, 44 p. text.

Barnolas, A., Chiron, J. C., and Guérangé, B., 1996, Synthèse géologique et géophysique des Pyrénées. Volume 1 : Introduction, Géophysique, Cycle Hercynien: Bureau de Recherches Géologiques et Minières, Orléans - Instituto Tecnológico Geominero de España, Madrid, 729 p.

Bengtson, S., Conway Morris, S., Cooper, B.J., Jell, P.A., and Runnegar, B.N., 1990, Early Cambrian fossils from south Australia: Memoirs of the Association of Australasian Palaeontologists, v. 9, p. 1–364.

Bischoff, C.G.O., 1989, Byroniida new order from early Palaeozoic strata of eastern Australia (Cnidaria, thecate scyphopolyps): Senkenbergiana Lethaea, v. 59, p. 275–327.

Casas JM, and Palacios T (2012) First biostratigraphical constraints on the pre–Upper Ordovician sequences of the Pyrenees based on organic-walled microfossils. Comptes Rendus Géosciences, v. 344, p. 50–56.

Casas, J.M., Álvaro, J.J., Clausen, S., Padel, M., Puddu, C., Sanz-López, J., Sánchez-García, T., Navidad, M., Castiñeiras, P., and Liesa, M., 2019. Palaeozoic basement of the Pyrenees. In: C. Quesada and J. T. Oliveira (eds.), The Geology of Iberia: A Geodynamic Approach, Regional Geology Reviews, vol. 2, p. 229–259.

Cavet, P., 1957, Le Paléozoïque de la zone axiale des Pyrénées orientales françaises entre le Roussillon et l'Andorre : Bulletin du Service de la Carte Géologique de France, v. 55, p. 303–518.

Clausen, S., Javier Álvaro, J.J., Devaere, L., Ahlberg, P., and Babcock, L.E., 2015, The Cambrian explosion: Its timing and stratigraphic setting: Annales de Paléontologie, v. 101, p. 153–160.

Cochelin, B., Chardon, D., Denèle, Y., Gumiaux, C., and Le Bayon, B., 2017, Vertical strain partitioning in hot Variscan crust: Syn-convergence escape of the Pyrenees in the Iberian-Armorican syntax. Bulletin de la Société géologique de France, v. 188, 39.

Cochelin, B., Lemirre, B., Denèle, Y., De Saint Blanquat, M., Lahfid, A., and Duchêne, S., 2018, Structural inheritance in the Central Pyrenees: the Variscan to Alpine tectonometamorphic evolution of the Axial Zone. Journal of the Geological Society, London, v. 175, p. 336–351.

Debrenne, F., Gandin, A., Courjault-Radé, P., 2002. Facies and depositional setting of the Lower Cambrian archaeocyath-bearing limestones of southern Montagne Noire (Massif Central, France). Bulletin de la Société géologique de France, v. 173, p. 533–546.

Denèle, Y., Laumonier, B., Paquette, J.-L., Olivier, P., Gleizes, G., and Barbey, P., 2014, Timing of granite emplacement, crustal flow and gneiss dome formation in the Variscan segment of the Pyrenees. Geological Society, London, Special Publications, v. 405, p. 265–287.

Devaere, L., Clausen, S., Monceret, E., Tormo, N., Cohen, H., and Vachard, D., 2014a, Lapworthellids and other skeletonised microfossils from the Cambrian Stage 3 of the northern Montagne Noire, southern France: Annales de Paléontologie, v. 100, p. 175–191.

Devaere, L., Clausen, S., Monceret, E., Vizcaïno, D., Vachard, D., and Genge, M.C., 2014b, The tommotiid *Kelanella* and associated fauna from the early Cambrian of southern Montagne Noire (France): implications for camenellan phylogeny: Palaeontology, v. 57, p. 979–1002.

Devaere, L., Clausen, S., Steiner, M., Álvaro, J.J., and Vachard, D., 2013, Chronostratigraphic and palaeogeographic significance of an early Cambrian microfauna from the Heraultia Limestone, northern Montagne Noire, France: Palaeontologia Electronica, v.16, 17A–91.

Gravestock, D.I., Alexander, E.M., Demidenko, Yu. E., Esakova, N.V., Holmer, L.E., Jago, J.B., Lin, T., Melnikova, L.M., Parkhaev, P.Yu., Rozanov, A.Yu., Ushatinskaya, G.T., Zang, W., Zhegallo, E.A., and Zhuravlev, A.Yu., 2001, The Cambrian biostratigraphy of the Stansbury Basin, South Australia: Transactions of the Palaeontological Institute, v. 282, p. 1–344.

Hinz-Schallreuter, I., Gozalo, R., and Liñán, E., 2007, New bradoriid arthropods from the Lower Cambrian of Spain: Micropaleontology, v. 53, p. 497–510.

Holmer, L.E., Popov, L.E. and Wrona, R., 1996, Early Cambrian lingulate brachiopods from glacial erratic of King George Island (South Shetland Islands), Antarctica, *in* Gazdzicki, A., ed., Palaeontological Results of the Polish Antarctic Expeditions. Part II: Palaeontologia Polonica, v. 55, p. 37–50.

Holmer, L.E., Stolk, S.P., Skovsted, C.B., Balthasar, U., and Popov, L., 2009, The enigmatic Early Cambrian Salanygolina – a stem group of rhynchonelliform chileate brachiopods?: Palaeontology, v. 52, 1–10.

Hou, X.-G., Siveter, D.J., Williams, M., and Xiang-Hong, F., 2001, A monograph of the bradoriid arthropods from the Lower Cambrian of SW China: Earth and Environmental Science Transactions of the Royal Society of Edinburgh, v. 92, p. 347–409.

Janussen, D., Steiner, M., and Maoyan, Z., 2002, New well-preserved scleritomes of Chancelloridae from the early Cambrian Yuanshan Formation (Chengjiang, China) and the middle Cambrian Wheeler Shale (Utah, USA) and paleobiological implications: Journal of Paleontology, v. 76, p. 596–606.

Kouchinsky, A., Bengtson, S., Clausen, S., Gubanov, A., Malinky, J.M., and Peel, J.S., 2011, A middle Cambrian fauna of skeletal fossils from the Kuonamka Formation, northern Siberia: Alcheringa, v. 35, p. 123–189.

Kouchinsky, A., Bengtson, S., Clausen, S., and Vendrasco, M.J., 2015, An early Cambrian fauna of skeletal fossils from the Emyaksin Formation, northern Siberia: Acta Palaeontologica Polonica, v. 60, p. 421–512.

Landing, E., 1988, Lower Cambrian of Eastern Massachusetts: Stratigraphy and small shelly fossils: Journal of Paleontology, v. 62, p. 661–695.

Laumonier, B., 1998, Les Pyrénées centrales et orientales au début du Paléozoïque (Cambrien sl): évolution paléogéographique et géodynamique: Geodinamica Acta, v. 11, p. 1–11.

Laumonier, B., 2015, Les Pyrénées alpines sud-orientales (France, Espagne) – essai de synthèse: Revue de Géologie pyrénéenne, v. 2, p. 1–44.

Laumonier, B., Marignac, C., and Kister, P., 2010. Polymétamorphisme et évolution crustale dans les Pyrénées orientales pendant l'orogenèse varisque au Carbonifère supérieur. Bulletin de la Société géologique de France, 181, 411–428.

Laumonier, B., Abad, A., Alonso, J.L., Baudelot, S., Bresiére, G., Besson, M., and Centéne, A., 1996, Cambro-ordovicien, *in* Barnolas, A., Chiron, J. C., and Guérangé, B., eds., Synthèse Géologique et Géophysique des Pyrénées. Volume 1 : Introduction, Géophysique, Cycle Hercynien: Bureau de Recherches Géologiques et Minières, Orléans – Instituto Tecnológico Geominero de España, Madrid, p. 157–209.

Laumonier, B., Autran, A., Barbey, P., Cheilletz, A., Baudin, T., Cocherie, A., and Guerrot, C., 2004, Conséquences de l'absence de socle cadomien sur l'âge et la signification des séries pré–varisques (anté–Ordovicien supérieur) du sud de la France (Pyrénées, Montagne Noire): Bulletin de la Société géologique de France, v. 175, p. 643–656.

Laumonier, B., Calvet, M., Wiazemsky, M., Barbey, P., Marignac, C., Lambert, J., Lenoble, J.L., 2015a, Carte géologique de la France, Feuille de Céret (1096): Bureau de Recherches Géologiques et Minières, Orléans, France, scale 1/50000, 1 sheet, 164 p. text.

Lemirre, B., Cochelin, B., Duchene, S., de Saint Blanquat, M., and Poujol, M., 2019, Origin and duration of late orogenic magmatism in the foreland of the Variscan belt (Lesponne-Chiroulet-Neouvielle area, French Pyrenees): Lithos, v. 336–337, p. 183–201.

Lescuyer, J.L., and Cocherie, A., 1992, Datation sur monozircons des metadacites de Sériès. Arguments pour un âge protérozoïque terminal des "schistes X" de la Montagne Noire (Massif Central français): Comptes Rendus de l'Académie des Sciences, Paris, Série 2, v. 314, p. 1071–1077.

Li, G., and Holmer, L.E., 2004, Early Cambrian lingulate brachiopods from the Shaanxi Province, China: GFF, vol. 126, p. 193–211.

Malinky, J., and Skovsted, C.B., 2004, Hyoliths and small shelly fossils from the Lower Cambrian of North-East Greenland: Acta Palaeontologica Polonica, v. 49, p. 551–578.

Martínez Catalán, J.R., Arenas, R., Díaz García, F., González Cuadra, P., Gómez-Barreiro, J., Abati, J., Castiñeiras, P., Fernández-Suárez, J., Sánchez Martínez, S., Andonaegui, P., González Clavijo, E., Díez Montes, A., Rubio Pascual, F.J., and Valle Aguado, B., 2007, Space and time in the tectonic evolution of the northwestern Iberian Massif: Implications for the Variscan belt, *in* Hatcher, R.D., Jr., Carlson, M.P., McBride, J.H., and Martínez Catalán, J.R., eds., 4-D Framework of Continental Crust: Geological Society of America Memoir 200, p. 403–423.

Menéndez, S., Perejón, A., and Moreno-Eiris, E., 2015, Late Ovetian (Cambrian Series 2, Stage 3) archaeocyathan biostratigraphy of Spain; Annales de Paléontologie, v. 101, p. 161–166.

Olivier, P., Gleizes, G., Paquette, J.L., and Munoz-Saez, C., 2008, Structure and U–Pb dating of the Saint-Arnac pluton and the Ansignan charnockite (Agly Massif): a cross-section from the upper to the middle crust of the Variscan Eastern Pyrenees: Journal of the Geological Society, London, v. 165, p. 41–152.

Padel, M., Álvaro, J.J., Casas, J.M., Clausen, S., Poujol, M., and Sánchez-García, T., 2018a, Cadomian volcanosedimentary complexes across the Ediacaran–Cambrian transition of the Eastern Pyrenees, southwestern Europe: International Journal of Earth Sciences, v. 107, p. 1579–1601.

Padel, M., Álvaro, J.J., Clausen, S., Guillot, F., Poujol, M., Chichorro, M., Monceret, E., Pereira, M.F., and Vizcaïno, D., 2017, U–Pb laser ablation ICP-MS zircon dating across

the Ediacaran–Cambrian transition of the Montagne Noire, southern France: Comptes Rendus Geoscience, v. 349, p. 380–390.

Padel, M., Clausen, S., Álvaro, J.J., and Casas, J.M., 2018b, Review of the Ediacaran–Lower Ordovician (pre–Sardic) stratigraphic framework of the Eastern Pyrenees, southwestern Europe: Geologica Acta, v. 16, p. 339–355

Parkhaev, P.Y., 2004, Malacofauna of the Lower Cambrian Bystraya formation of eastern Transbaikalia: Paleontological Journal, v. 38, p. 590–608.

Paterson, J.R., Skovsted, C.B., Brock, G.A. and Jago, J.B., 2007, An early Cambrian faunule from the Koolywurtie Limestone Member (Parara Limestone), Yorke Peninsula, South Australia and its biostratigraphic significance: Memoirs of the Association of Australasian Palaeontologists, v. 34, p. 131–146.

Pereira, M.F., Castro, A., Chichorro, M., Fernández, C., Díaz-Alvarado, J., Martí, J., and Rodríguez, C., 2014, Chronological link between deep-seated processes in magma chambers and eruptions: Permo–Carboniferous magmatism in the core of Pangaea (Southern Pyrenees): Gondwana Research, v.25, p. 290–308.

Perejón, A., Moreno-Eiris, E., and Abad, A., 1994, Montículos de arqueociatos y calcimicrobios del Cámbrico inferior de Terrades, Gerona (Pirineo oriental): Boletín de la Real Sociedad Española de Historia Natural, Sección Geológica, v. 89, p. 55–95.

Peng, S.C., Babcock, L.E., and Cooper, R.A., 2012, The Cambrian Period, *in* Gradstein, F.M., Ogg, J.G., Schmitz, M.D., and Ogg, G.M., eds., The Geologic Time Scale 2012, vol. 2: Elsevier BV, Amsterdam, p. 437–488.

Porter, S.M., 2008, Skeletal microstructure indicates chancelloriids and halkieriids are closely related: Palaeontology, v. 51, p. 865–879.

Pouclet, A., Álvaro, J.J., Bardintzeff, J.M., Imaz, A.G., Monceret, E., and Vizcaïno, D., 2016, Cambrian–early Ordovician volcanism across the South Armorican and Occitan Domains

of the Variscan Belt in France: Continental break-up and rifting of the northern Gondwana margin: Geoscience Frontiers, v. 8, p. 25–64.

Pujadas, J., Casas, J.M., Muñoz, J.A., Sabat, F., 1989. Thrust tectonics and Paleogene syntectonic sedimentation in the Empordà area, southeastern Pyrenees. Geodinamica Acta, v. 3, p. 195–206.

Rigby, J.K., 1978, Porifera of the Middle Cambrian Wheeler Shale, from the Wheeler Amphitheater, House Range, in western Utah: Journal of Paleontology, v. 52, p. 1325–1345.

Romero, P. & Schimmel, M. 2018. Mapping the basement of the Ebro Basin in Spain with seismic ambient noise autocorrelations. Journal of Geophysical Research: Solid Earth, 123, 5052–5067.

Siveter, D. J. and Williams, M., 1997, Cambrian bradoriid and phosphatocopid arthropods of North America: Special Papers in Palaeontology, v. 57, 1–69.

Siveter, D.J., Williams, M., Peel, J.S., and Siveter, D.J., 1996, Bradoriida (Arthropoda) from the early Cambrian of North Greenland: Transactions of the Royal Society of Edinburgh: Earth Sciences, v. 86, p. 113–121.

Skovsted, C.B., 2004, Mollusc fauna of the Early Cambrian Bastion Formation of north-east Greenland: Bulletin of the Geological society of Denmark, v. 51, p. 11–37.

Skovsted, C.B., Brock, G.A., and Paterson, J.R., 2006, Bivalved arthropods from the Lower Cambrian Mernmerna Formation, Arrowie Basin, South Australia and their implications for the identification of Cambrian ‘small shelly fossil’: Memoirs of the Association of Australasian Palaeontologists, v. 32, p. 7–41.

Skovsted, C.B., and Peel, J.S., 2011, *Hyolithellus* in life position from the lower Cambrian of North Greenland: Journal of Paleontology, v. 85, p. 37–47.

Steiner, M., Li, G., Qian, Y., Zhu, M., and Erdtmann, B.D., 2007, Neoproterozoic to early Cambrian small shelly fossil assemblages and a revised biostratigraphic correlation of the Yangtze Platform (China): Palaeogeography, Palaeoclimatology, Palaeoecology, v. 254, p. 67–99.

Thoral, M., 1935, Contribution à l'étude géologique des Monts de Lacaune et des terrains cambriens et ordoviciens de la Montagne Noire: Bulletin du Service de la Carte géologique de la France, v. 192, 307 p.

Thoral, M., 1935, Contribution à l'étude paléontologique de l'Ordovicien inférieur de la Montagne Noire et révision sommaire de la faune cambrienne de la Montagne Noire: Montpeller, Imprimerie de la Manufacture de la Charité, 362 p.

Topper, T.P., Skovsted, C.B., Brock, G.A., and Paterson, J. R., 2007, New bradoriids from the lower Cambrian Mernmerna Formation, South Australia: systematics, biostratigraphy and biogeography: Memoirs of the Association of Australasian Palaeontologists, v. 33, p. 67–100.

Topper, T. P., Brock, G. A., Skovsted, C. B., and Paterson, J. R., 2009. Shelly Fossils from the Lower Cambrian '*Pararaia bunyerooensis*' Zone, Flinders Ranges, South Australia. Australasian Palaeontological Memoirs, v. 37, p. 199–246.

Topper, T.P., Skovsted, C.B., Harper, D.A., and Ahlberg, P., 2013, A bradoriid and brachiopod dominated shelly fauna from the Furongian (Cambrian) of Västergötland, Sweden: Journal of Paleontology, v. 87, p. 69–83.

Vannier, J., Williams, M., Álvaro, J.J., Vizcaïno, D., Monceret, S., and Monceret, E., 2005, New Early Cambrian bivalved arthropods from southern France: Geological Magazine, v. 142 , p. 751–763.

Williams, M., Siveter, D.J., Hinz-Schallreuter, I., and Melnikova, L., 1994, On *Cambria sibirica* Neckaja and Ivanova: A Stereo-Atlas of Ostracod Shells, v. 21, p. 9–12.

Williams, M., Siveter, D.J., Popov, L.E., and Vannier, J.M., 2006, Biogeography and affinities of the bradoriid arthropods: cosmopolitan microbenthos of the Cambrian seas: Palaeogeography, Palaeoclimatology, Palaeoecology, v. 248, p. 202–232.

Wrona, R., 2004, Cambrian microfossils from glacial erratics of King George Island, Antarctica: Acta Palaeontologic Polonica, v. 49, p. 13–56.

Yang, B., 2014, Cambrian small shelly fossils of South China and their application in biostratigraphy and palaeobiogeography: Berlin, Doctoral dissertations of the Freie Universität Berlin, 164 p.

Zhang, X.G., 2007, Phosphatized bradoriids (Arthropoda) from the Cambrian of China: Palaeontographica Abteilung A, v. 281, p. 93–173.

Zhang, Z., Zhang, Z., Holmer, L.E., and Li, G., 2015, First report of linguloid brachiopods with soft parts from the lower Cambrian (Series 2, Stage 4) of the Three Gorges area, South China: Annales de Paléontologie, v. 101, p. 167–177.

Figure Caption

Figure 1. Sketch map of the tectonostratigraphic units of the westernmost Variscan realm (modified after Martínez-Catalán et al. 2007, Ballèvre et al. 2009, Álvaro et al., 2010; Pouclet et al., 2016). AM: Armorican Massif; C: Cornwall; CELA: Cantabrian-Ebroan Land Area; CZ: Cantabrian Zone; CIZ: Central Iberian Zone; GTMZ: Galicia-Trás-os Montes Zone; MC: French Central Massif; MN: Montagne Noire; OM: Ossa-Morena Zone; PZ: Pyrenean Domain; SAD: South-Armorican Domain; OD: Occitan Domain; SPZ: South-Portuguese Zone; RHZ: Rheno-Hercynian Zone; STZ: Saxo-Thuringian Zone; WALZ: West Asturian-Leonese Zone.

Figure 2. Geological sketches of the Pyrenees. A. Location and main structural domains of the Pyrenees, southwestern Europe. B. Main Alpine tectonostratigraphic units of the Pyrenees

(after Baudin et al., 2008; Laumonier, 2015) with location of the Terrades (or La Salut) unit studied herein (inset box, magnified in Figure 3).

Figure 3. Simplified geological map of the Terrades inlier (La Salut unit) and surrounding area with location of the studied section (after Baudin et al., 2008).

Figure 4. Stratigraphic comparison between the Ediacaran–Cambrian (part.) successions of the eastern Pyrenees and the Montagne-Noire (modified from Padel et al.,2018b after Devaere et al., 2013, 2014a, b).

Figure 5. Lithological log of the Cambrian succession outcropping on the left bank of the Salt del Barral stream, north of Terrades (Gerona Province, Spain), with location of studied samples (modified from Perejón et al., 1994).

Figure 6. Bradoriid sp. A from sample TE2F. Articulated, partly broken valves of specimen USTL(CTE2F_009): left lateral view (1), oblique dorsal view (2), ventral view (3), oblique anterior view (4) with detail of the spine in (5). Terminology: *adc*, anterodorsal cusp; *pdl*, posterodorsal lobe; *ads*, anterodorsal spine; *vr*, ventral ridge.

Figure 7. Bradoriid sp. B from sample TE2F. **1**. Deformed, subamplete, articulated valves of specimen USTL (CTE2F_010): lateral view. **2-4**. Articulated, partly opened valves of specimen USTL (DTE2F_010): right lateral view (2), oblique dorsal view (3), oblique ventral view (4). Figs. 5-8. Partly preserved, articulated valves of specimen USTL (CTE2F_004): right lateral

view (5), oblique dorsal view (6), view of anterior lobe (7) area in square magnified in (8) showing pustulose and polygonal ornaments. **9-12**. Articulated valves of specimen USTL (CTE2F_012): oblique posterior view (9), oblique dorsal view (10), right lateral view (11), and ventral view (12). **13-14**. Articulated valves of specimen USTL (JTE2F_12): right lateral view (13), dorsal view (14) showing highly projecting nodes. **15-16.** Articulated valves of specimen USTL (JTE2F_002): dorsal view (15), area in square magnified in (16) to show spinose ornamentation. Terminology: *cs*, cardinal spine; *adr*, anterodorsal ridge; *adn*, anterodorsal node; *pdn*, posterodorsal node; *cr*, connecting ridge; *lr*, lateroadmarginal ridge. Arrows points the anterodorsal ridge.

Figure 8. Bradoriid sp. B from sample TE2F. **1-3**. Articulated, slightly open valves of specimen USTL (DTE2F_006): right lateral view (1), oblique dorsal view (2), oblique ventral view (3). **4-7.** Articulated, closed valves of specimen USTL (DTE2F_014): left lateral view (4) area in square magnified in (7), oblique dorsal view (5), dorsal view (6). **8-10**. Articulated valves (antero dorsal corner broken) of specimen USTL (DTE2F_002): left lateral view (8), oblique dorsal view (9), dorsal view (10). **11-12,16**. Broken valve (specimen USTL (CTE2F_005)): lateral views (11-12), with detail of a broken spine (16). **13-15**. Articulated valves with broken ventral margin of specimen USTL (CTE2F_008): dorsal view (13), right? lateral view (14), area in square magnified in (15) to show spinose and polygonal ornaments. **17-18**. Incomplete specimen USTL (DTE2F_005): antero-lateral view (17) showing well developed admarginal convex area, squared area showing detail of spinose ornament in (18). **19-22**. Deformed, crinkled specimen USTL (CTE2F_014) with slightly broken articulated valves: lateral view (19), area in square magnified in (20) to show detail of pustulose and polygonal ornament, oblique dorsal view (21), oblique ventral view (22).

Figure 9. Bradoriids sp. B from sample TE2F. **1-2**. Internal mould of articulated valve of specimen USTL (CTE2F_003): left lateral view (1) and dorsal view (2). **3-6**. Articulated, subamplete valves of specimen USTL (DTE2F_001): right? lateral view (3), oblique dorsal view (4), area in square magnified in (5) to show superficial polygonal meshwork, oblique view (6). **7-9.** Articulated valves of specimen USTL (DTE2F_013): left lateral view (7), oblique dorsal view (8), ventral view (9). 10-12. Strongly flattened Specimen USTL (BTE2F_009): lateral view (10), oblique view (11), detail of the flattened posterior lobe (12).

Figure 10. Specimens of *P.* cf. *subangulata* from sample TE2F. **1-2**. Specimen USTL (GTE2F_007) in basal view (1) and apertural view (2). **3-4**. Specimen USTL (GTE2F_008) in basal view (3) and apertural view (4). **5-6**. Specimen USTL (GTE2F_013) in basal view (5) and apertural view (6). **7-8**. Specimen USTL (GTE2F_015) in basal view (7) and apertural view (8). **9-10**. Specimen USTL (GTE2F_017) in dorsal view (9) and apertural view (10). **11-12**. Specimen USTL (GTE2F_010) in basal view (11) and lateral view (12).

Figure 11. Specimens of *Eoobolus* sp. from samples TE1E and TE2F. **1-2.** Specimen USTL (TE1E-11-2): lateral (1) and apical (2) views. **3**. Specimen USTL (GTE2F_018) in lateral view. **4-8**. Dorsal valve of specimen USTL (ATE1E_009): inner view (4) showing pseudointerarea (*Pi*), posterior portion of the visceral platform (*Pvp*), median projection of the visceral platform (*Mp*) and anterior portion of the visceral platform (*Avp*), with detail of pseudointerarea (6) and second central muscle scars (*2c*) and polygonal structures (8), anterior view (5), area in square magnified in (7) showing first lateral muscle scars (*1l*) and elevated pseudointerarea. **9-11**. Ventral valve of specimen USTL (BTE1E_001): anterior oblique view (9), area in square magnified in (10) showing detail of pseudointerarea, inner view (11). **12-15**. Ventral valve of specimen USTL (H TE2F_001): anterior view (12), inner view (13) with detail of apical region

(14), area in square magnified in (15) showing detail of pedicle nerves (*Pn*) and polygonal structures.

Figure 12. Specimens of *Eoobolus* sp. from samples TE1E and TE1D. **1-2, 4**. Dorsal valve of specimen USTL (TE1E-15-12): lateral oblique view (1) showing *vascula lateralia* (*Vl*) and median depression (*Md*); inner view (2); anterior view (4). **3, 5-6**. Dorsal valve of specimen USTL (BTE1E_007): inner view (3) with median ridge (*Mr*), area in square magnified in (6) showing second central muscle scars (*2c*), oblique anterior view (5). **7-9**. Dorsal valve of specimen USTL (BTE1E_008): inner view (7) magnified in (8) showing detail of first central muscle (*1c*) and first lateral muscle (*1l*) scars, external apical view (9) showing rounded shape of larval shell. **10-11**. Ventral valve of specimen USTL (HTE2F_001): inner view (10) showing *vascula lateralia (Vl*), area in square magnified in (11) showing detail of first central muscle scars (*1c*). **12-14**. Dorsal valve of specimen USTL (TE1E-1-6): inner view (12), area in square magnified in (13) showing detail of third central muscle scars (*3c*), anterior oblique view (14). **15-16**. Ventral valve of specimen USTL (TE1D-2-4): inner view (15), area in square magnified in (16) showing detail of *vascula lateralia (Vl*). **17-18**. Ventral valve of specimen USTL (BTE1E_013): inner view (17), area in square magnified in (18).

Figure 13. Specimens of *Eoobolus* sp. from samples TE1E and TE2F. **1-2**. Dorsal valve of specimen USTL (TE1E-3-13): inner view (1), area in square magnified in (2) showing detail of radiating faint ridges. **3-5**. Dorsal valve of specimen USTL (TE1E-11-3): inner (3) and lateral (4) views, area in square magnified in (5) showing detail or radiating fine ridges. **6-10**. Ventral valve of specimen USTL (TE1E-7-2_017): inner view (6), anterior view (7) showing emarginature, area in square magnified in (8) showing detail of polygonal structures between pseudointerarea and shell floor, lateral view (9), area in square magnified in (10) showing detail

of columnar microstructure. **11-12**. Dorsal valve of specimen USTL (TE 1E-7-6): oblique posterior view (11), area in square magnified in (12) showing detail of larval shell. **13-15**. Specimen USTL (TE1E-11-1): lateral view (13), posterior view showing median sulcus (14), external view (15). **16-20**. Juvenile articulated specimen USTL (GTE2F_003): dorsal view (16), area in square magnified in (19) showing detail of pustulose ornament on post-larval shell; posterior view (17) detailed in (18) showing U-shaped emarginature, area in square magnified in (20) showing detail of pitted ornament on larval shell.

Figure 14. Specimens of *Microcornus* cf. *pelitus* from sample TE2F. **1-2**. Specimen USTL (FTE2F_007): dorsal view (1) and apertural view (2). **3-5**. Specimen USTL (FTE2F_009): apertural view (3), dorsal view (4), area in square magnified in (5) showing detail of weak polygonal patterns on the surface of the internal mould. **6**. Specimen USTL (FTE2F_006) in lateral view. **7**. Specimen USTL (FTE2F_008) in lateral view.

Figure 15. Specimens of *Cupitheca* sp. from sample TE2F. **1-2**. Specimen USTL (FTE2F_015): lateral (1) and apical (2) views. **3, 5-6, 9, 11**. Specimen USTL (FTE2F_12): lateral view (3) with upper area in square magnified in (5) showing the faint transverse striations and lower area in square magnified in (6) showing the pits on the external coating, apical view (9) with area in square magnified in (11) showing the phosphatics rods and corresponding pits. **4, 10**. Specimen USTL (FTE2F_001): apical view (4), area in square magnified in (10) showing detail of phosphatic rods. **7-8**. Specimen USTL (FTE2F_13): lateral (7) and apical (8) views.

Figure 16. Type A sclerites of *Kelanella altaica* from samples TE2F and TE1E. **1-3**. Specimen USTL (JTE2F_016): lateral views (1-2) and upper view (3). **4-6, 10-12**. Specimen

USTL (TE1E-9-3): lateral view (4), area in square magnified in (12) showing detail of the gridded ornament, lateral views showing the duplicature (5-6) area in square magnified in 11, apertural view (10). **7-9** Specimen USTL (JTE2F_005): apertural view (7), lateral views (8-9).

Figure 17. Type B sclerites of *Kelanella altaica* from sample TE1E. Specimen USTL (TE1E 9-1): lateral views (**1-3**), area in square magnified in **4**, arrow pointing deep sulcus, apical view (**5**), area in square magnified in (**6**) and (**7**), showing weak growth lines.

Figure 18. Type C sclerites of *Kelanella altaica* from samples TE1D, TE2F and TE1E. **1-2, 7, 12**. Specimen USTL (TE1D-2-6): lateral view (1), oblique apical view (2), area in square magnified in (12), apertural view (7). **3-6**. Specimen USTL (TE1E-9-2): views of lateral facet (3), duplicature (4) and gridded facet (5), apical view (6). **8-10, 15**. Specimen USTL (TE1E-9-6): lateral views showing gridded facet (8), transversal septa (9), area in square magnified in (15) and duplicature (10). **11, 13-14**. Specimen USTL (KTE2F_003): apical view (11), lateral view showing gridded facet (13) and lateral facet (14).

Figure 19. Sclerites of *Kelanella altaica* from samples TE2F and TE1E. **1-4**. Type E. **1-3**. Specimen USTL (TE1E-10-2): lateral views of gridded and single lateral facets (1), duplicature and lateral facet (2) and gridded facet (3). 4. Specimen USTL (KTE2F_002) in lateral view showing gridded facet and single lateral facet. **5-6**. Specimen USTL (TE1E-9-7) (unrecognizable type): view of internal cavity with transverse septa (5), area in square magnified in (6) showing polygonal network on septa.

Figure 20. Chancelloriid sclerites from sample TE2F. 1-6: *Chancelloria*, sp. **1**. Specimen USTL (BTE2F_005) in abaxial view. **2-3**. Specimen USTL (TE2F_004) in abaxial view (2), area in square magnified in (3) showing detail of verruculose texture. **4**. Specimen USTL (ATE2F_012) in abaxial view. **5-6**. Specimen USTL (BTE2F_006) in abaxial view (5), area in square magnified in (6). **7-14**. *Allonnia tetrathallis*. **7-8**. Specimen USTL (ATE2F_013) 4+0 type in abaxial view (7) and oblique view (8). **9-10**. Specimen USTL (ATE2F_007) 5+0 type in abaxial view (9) and oblique view (10). **11-12**. Specimen USTL (ATE2F_008) 6+0 type in abaxial view (11) and oblique view (12). **13-14**. Specimen USTL (ATE2F_005) in abaxial view (13) and oblique view (14). 15-17: *Archiasterella charma*, Specimen USTL (ATE2F_009) in basal view (15) and lateral view (16), area in square magnified in (17) showing detail of verruculose texture.

Figure 21. Hyolithelminth tubes from samples TE2F and TE1E. **1-9**. *Hyolithellus* sp. **1-3**. Specimen USTL (TE1E-3-9): lateral view (1), adapical view (2) and apertural view (3). **4, 6-7**. Specimen USTL (TE1E-6-2): lateral oblique view (4), area in square magnified in (6) showing detail of transverse growth lines, view of the cross-section (7). **5, 8**. Specimen USTL (TE1E-6-14): lateral view (5) with arrow pointing to interrupted transverse rib, adapical view (8). **9.** Specimen USTL (TE1E-6-7) in lateral view, arrows pointing to interrupted transverse ribs. **10-28**. *Torellella*? sp. **19, 21, 27**. Specimen USTL (HTE2F_009): apertural view (19), area in square magnified in (27) showing detail of faint transverse ribs, lateral view (21). **10-13**. Specimen USTL (TE1E-12-8): lateral view (10), apertural view (11), area in square magnified in (13), apical view (12). **14-15**. Specimen USTL (HTE2E_010): apertural view (14), lateral view (15). **20, 22**. Specimen USTL (HTE2F_002): lateral view (20) and apertural view (22). **16-18**. Specimen USTL (TE1E-3-4): lateral view (16), apical view (17), apertural view (18). **23-25**. Specimen USTL (TE1E-13-2): apertural view (23), lateral views (14-25) with arrows

pointing to longitudinal ridge. **26, 28**. Specimen USTL (ITE2F_027): lateral view (26), area in square magnified in (28) showing detail of transverse ribs.

Figure 22. Specimens of *Rhombocorniculum cancellatum* from sample TE2F. **1-2, 7, 9.** Specimen USTL (ETE2F_006): lateral view (1), squared areas magnified in (7), and further in (9) showing detail of cancellate ornamentation, apertural view (2). **3**. Specimen USTL (ETE2F_008) in apertural view. **4, 8**. Specimen USTL (ETE2F_009): apertural view (4), area in square magnified in (8). **5-6**. Specimen USTL (ETE2F_007): apertural view (5), area in square magnified in (6).

Figure 23. Indeterminate subconical elements from samples TE2F. **1-3, 6, 9**. Specimen USTL (ITE2F_020): lateral view (1), area in square magnified in (9) showing detail of polygonal network and row of pustules, posterior view (2), area in square magnified in (6) showing detail of lamellae, basal view (3). 4-5. Specimen USTL (ITE2F_018): lateral view (4), area in square magnified in (5) showing detail of papillate structures. **7-8, 13-14**. Specimen USTL (ITE2F_015): basal view (8), oblique anterior view (13), area in square magnified in (7) showing detail of longitudinal furrows and pits, lateral view (14). **11,16**. Specimen USTL (ITE2F_014): lateral view (11) and basal view (16). **12.15**. Specimen USTL (ITE2F_013): lateral view (12), area in square magnified in (15) showing detail of longitudinal furrows and pits. **17-18, 20-21**. Specimen USTL (ETE2F_012): posterior view (17), area in square magnified in (20) showing detail of rows of pustules; lateral view (18), area in square magnified in (21) showing detail of spinose ornament. **10, 22, 25, 27**. Specimen USTL (ITE2F_024): oblique view (10), lateral view (22), area in square magnified in (25) showing detail of longitudinal rows of faint ridges, transversal view (27). **28**. Specimen USTL (ITE2F_002) in basal view. **23, 24, 29**. Specimen USTL (ITE2F_023): basal view (23), lateral view (24), area

in square magnified in (29) showing detail of polygonal structures. **19, 26**. Specimen USTL (ITE2F_003) in lateral view (19), area in square magnified in (26) showing detail of pustulose ornament at the apex.

Table 1. Measurements on ventral and dorsal valves of *Eoobolus*. L, W, Length and width of valve; Il, Iw, length and width of pseudointerarea; Vl, length of visceral platform; Ls, length of larval shell. MIN, minimum value; MAX, maximum value; N; number of values; S, standard deviation.

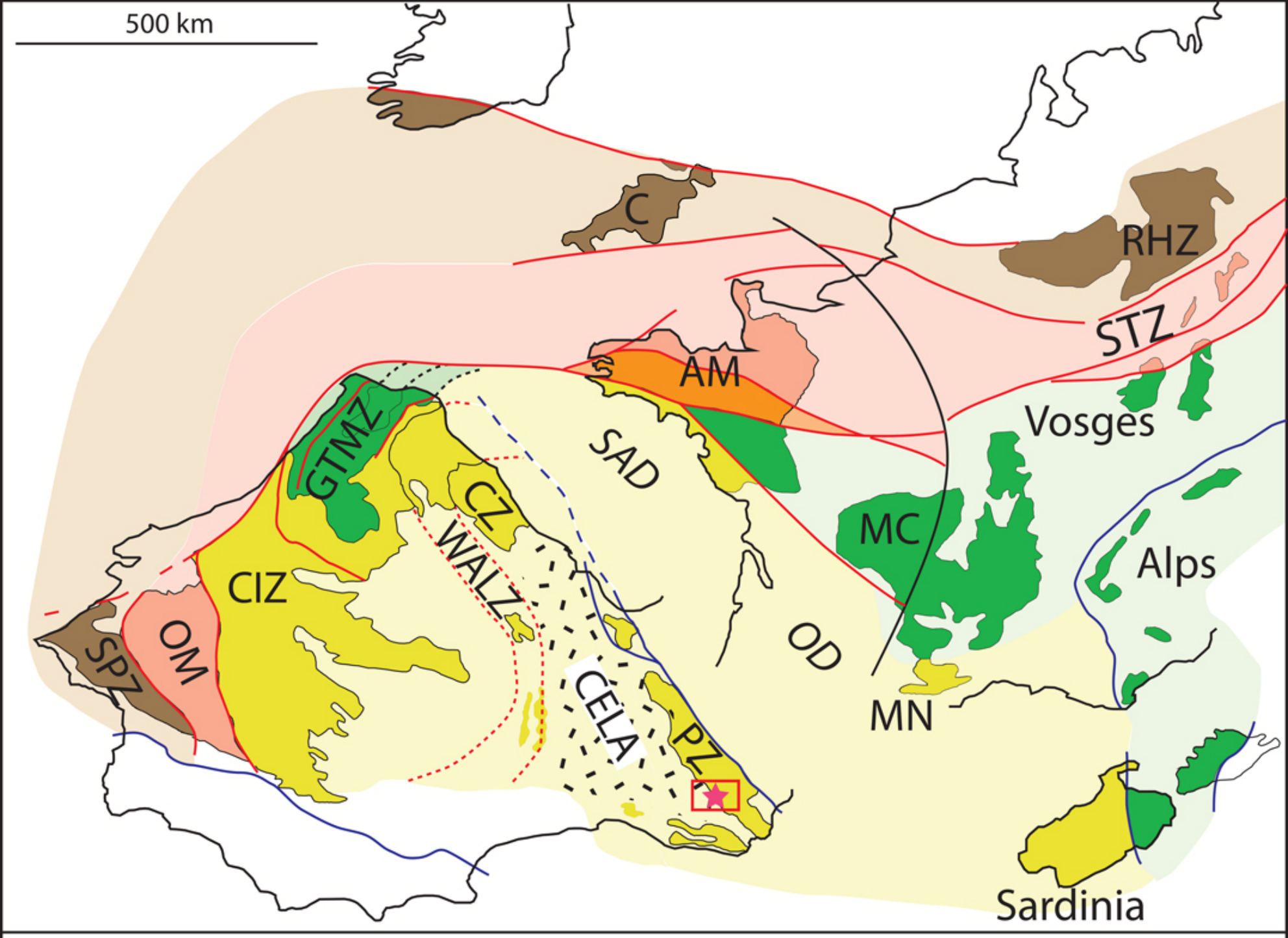
500 km
C
RHZ
STZ
AM
Vosges
GTMZ
SAD
CZ
WALZ
MC
Alps
CIZ
OM
SPZ
OD
CELA
PZ
MN
Sardinia
Northern Gondwana margin
Central Armorica terranes
Mid-German Rise and Léon
Allochthonous terranes of the Gondwana margin
Rheic terranes
Cantabrian-Ebroan Land area
Alpine and structures
Variscan
Study area

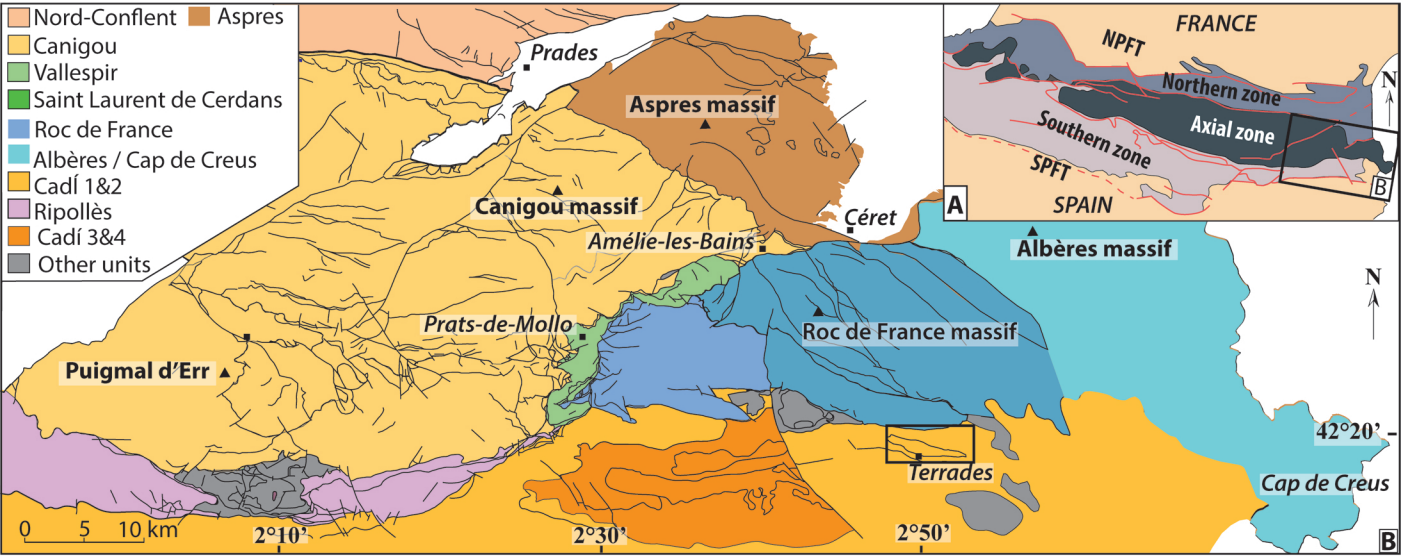
Nord-Conflent
Aspres
Canigou
Vallespir
Saint Laurent de Cerdans
Roc de France
Albères / Cap de Creus
Cadí 1&2
Ripollès
Cadí 3&4
Other units
Prades
Aspres massif
Canigou massif
Céret
Amélie-les-Bains
Albères massif
Prats-de-Mollo
Roc de France massif
Puigmal d'Err
Terrades
Cap de Creus
0 5 10 km
2°10'
2°30'
2°50'
42°20'
N
FRANCE
NPFT
Northern zone
Axial zone
Southern zone
SPFT
SPAIN
A
B

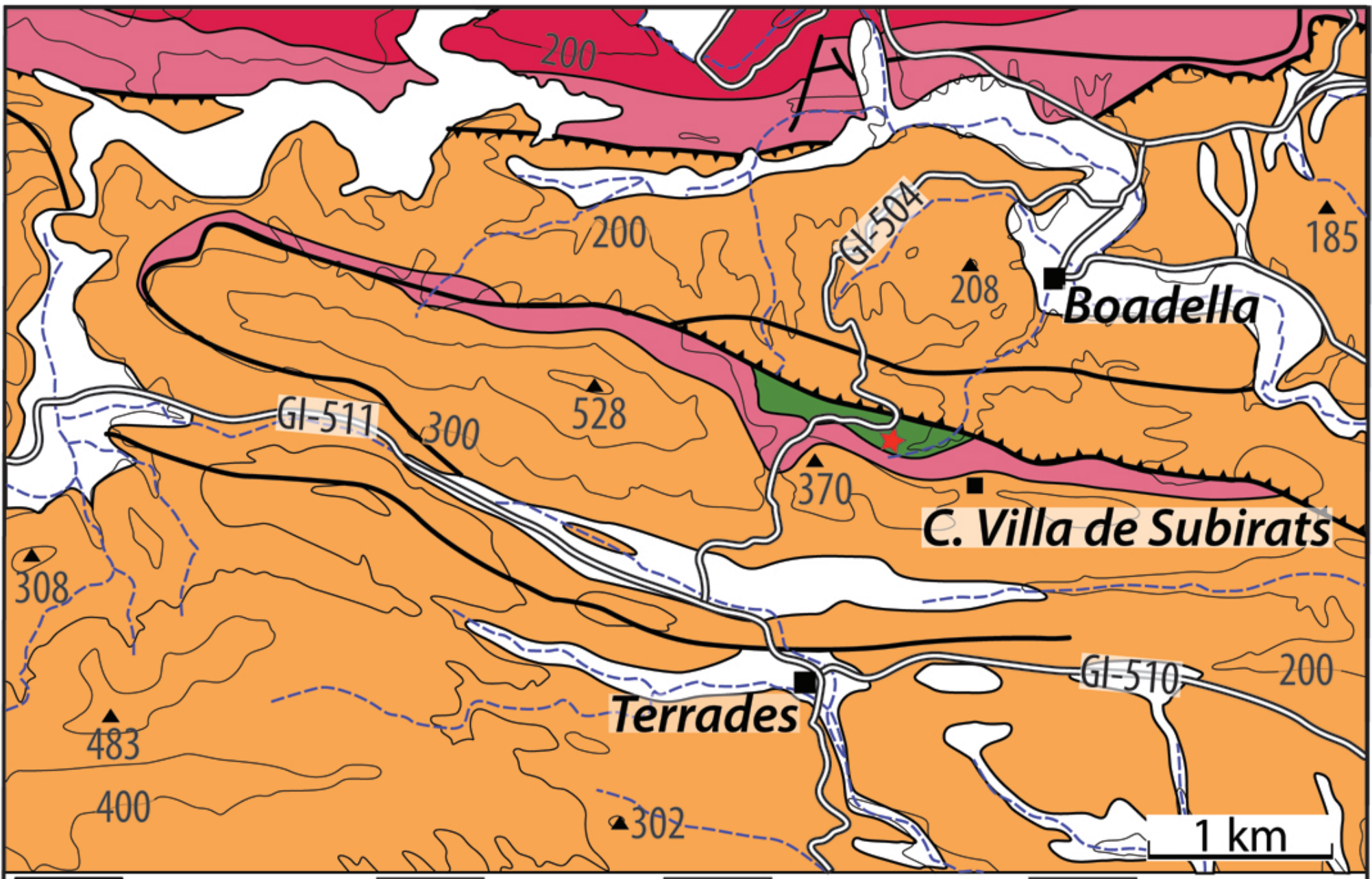
200
200
GI-504
208
185
Boadella
GI-511
300
528
370
C. Villa de Subirats
308
Terrades
GI-510
200
483
400
302
1 km
Quaternary
Eocene
Cretaceous
Cambrian
Carboniferous Granite
Faults
Studied section
Waterways
Contour lines
Roads

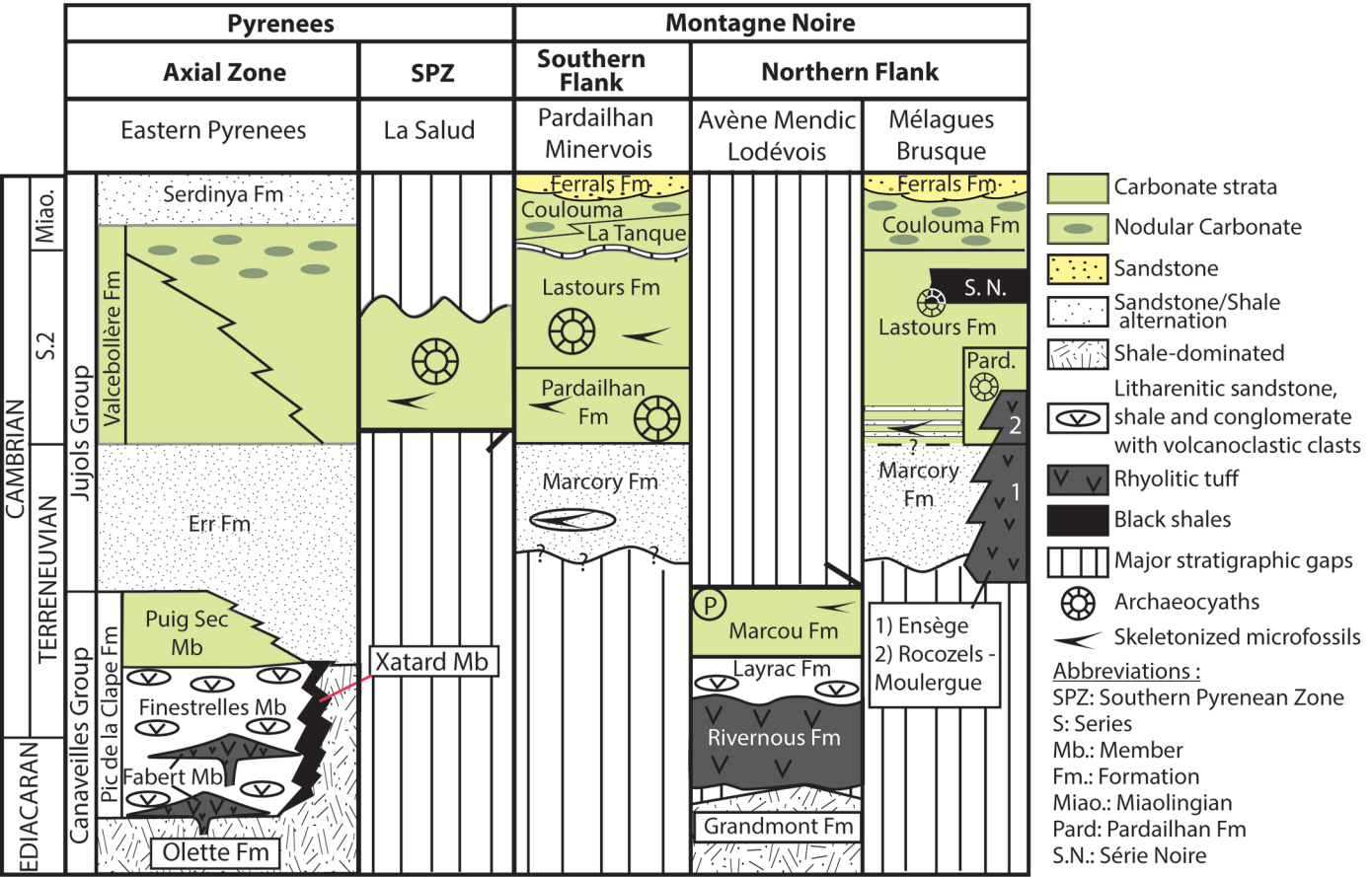
Pyrenees
Montagne Noire
Axial Zone
SPZ
Southern Flank
Northern Flank
Eastern Pyrenees
La Salud
Pardailhan Minervois
Avène Mendic Lodévois
Mélagues Brusque
CAMBRIAN
EDIACARAN
Miao.
S.2
TERRENEUVIAN
Jujols Group
Canaveilles Group
Serdinya Fm
Valcebollère Fm
Err Fm
Puig Sec Mb
Pic de la Clape Fm
Finestrelles Mb
Fabert Mb
Olette Fm
Xatard Mb
Ferrals Fm
Coulouma
La Tanque
Lastours Fm
Pardailhan Fm
Marcory Fm
Coulouma Fm
S. N.
Pard.
2
1
P
Marcou Fm
Layrac Fm
Rivernous Fm
Grandmont Fm
1) Ensège
2) Rocozels - Moulergue
Carbonate strata
Nodular Carbonate
Sandstone
Sandstone/Shale alternation
Shale-dominated
Litharenitic sandstone, shale and conglomerate with volcanoclastic clasts
Rhyolitic tuff
Black shales
Major stratigraphic gaps
Archaeocyaths
Skeletonized microfossils
Abbreviations :
SPZ: Southern Pyrenean Zone
S: Series
Mb.: Member
Fm.: Formation
Miao.: Miaolingian
Pard: Pardailhan Fm
S.N.: Série Noire

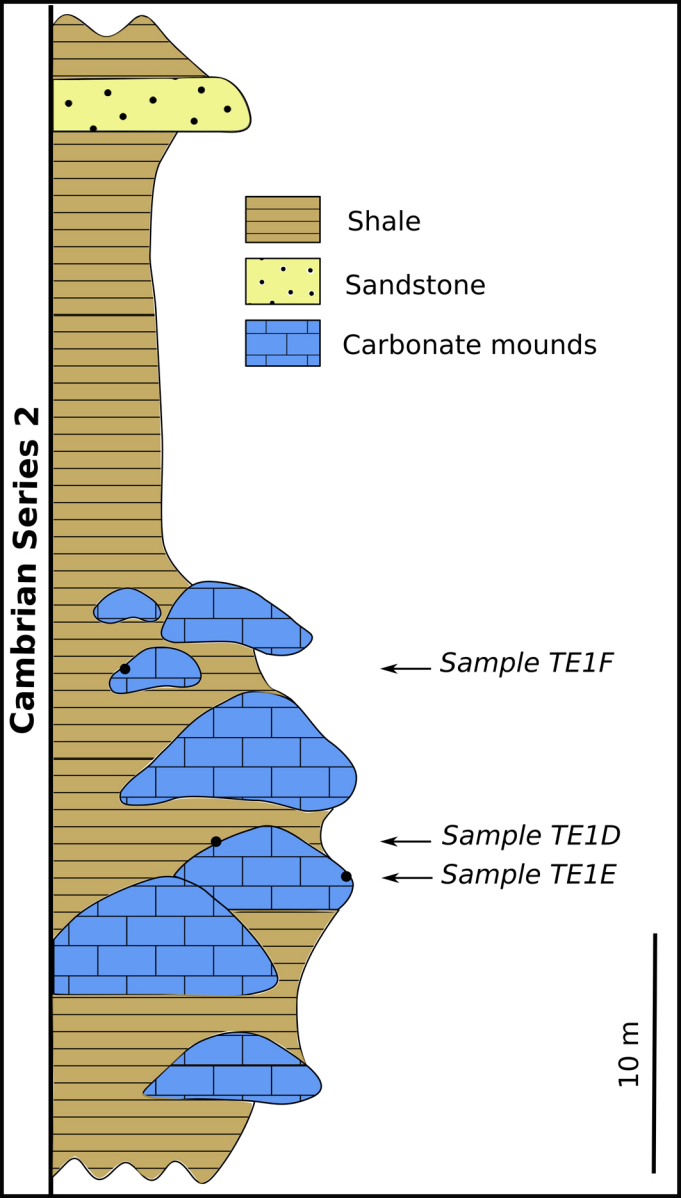
Cambrian Series 2
Shale
Sandstone
Carbonate mounds
Sample TE1F
Sample TE1D
Sample TE1E
10 m

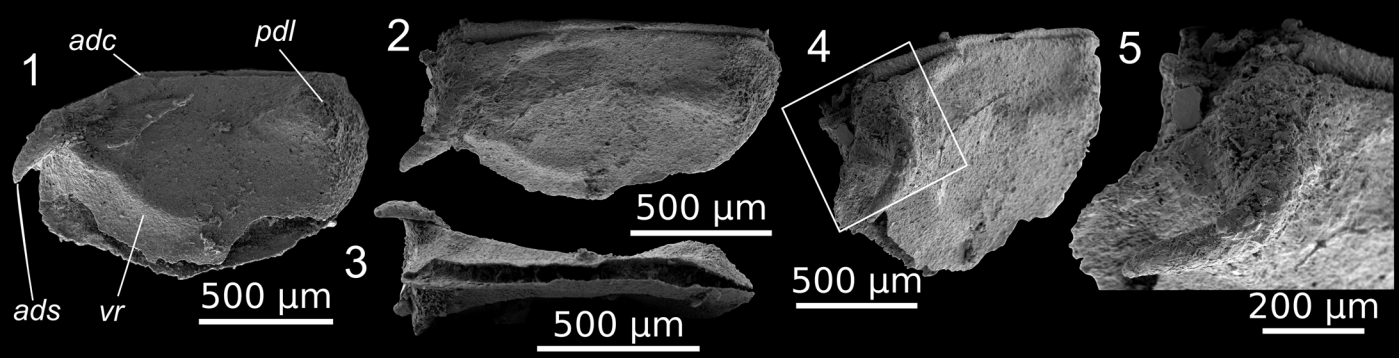
1
adc
pdl
ads
vr
500 µm
2
500 µm
3
500 µm
4
500 µm
5
200 µm

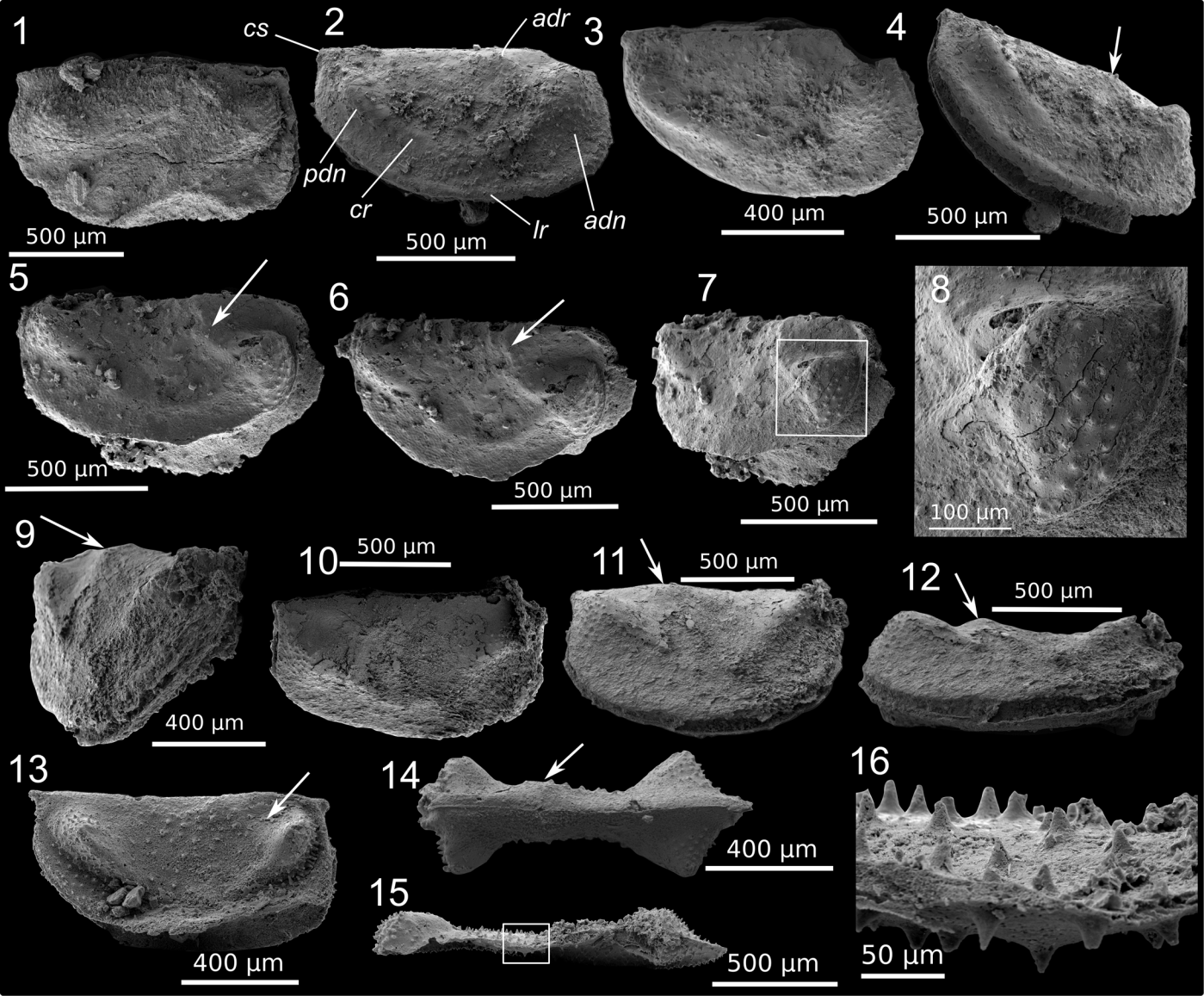
1
cs
2
adr
3
4
pdn
cr
lr
adn
500 µm
500 µm
400 µm
500 µm
5
6
7
8
500 µm
500 µm
500 µm
100 µm
9
10
11
12
400 µm
500 µm
500 µm
500 µm
13
14
15
16
400 µm
400 µm
500 µm
50 µm

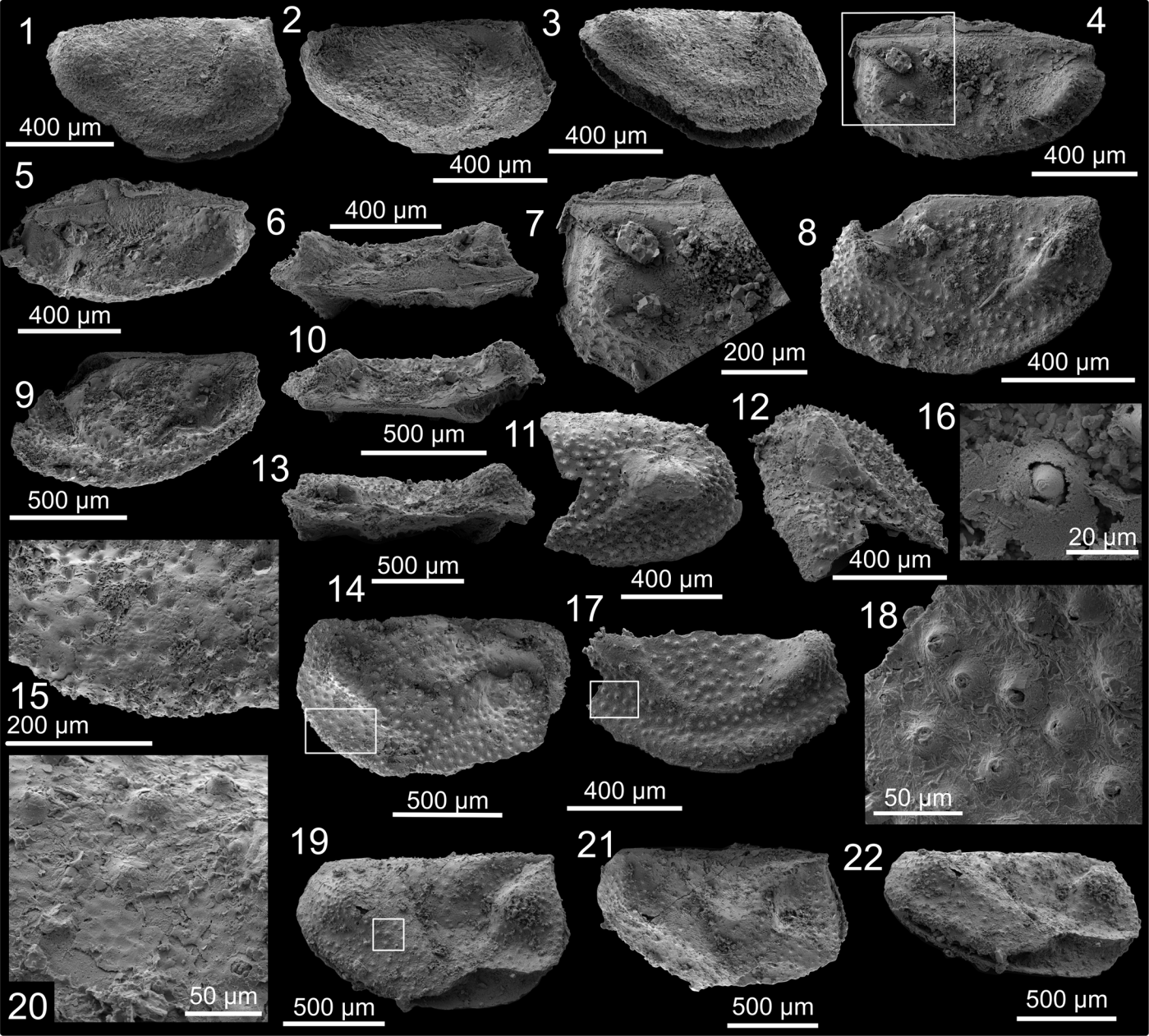
1
400 µm
2
400 µm
3
400 µm
4
400 µm
5
400 µm
6
400 µm
7
200 µm
8
400 µm
9
500 µm
10
500 µm
11
400 µm
12
400 µm
13
500 µm
14
500 µm
15
200 µm
16
20 µm
17
400 µm
18
50 µm
19
500 µm
20
50 µm
21
500 µm
22
500 µm

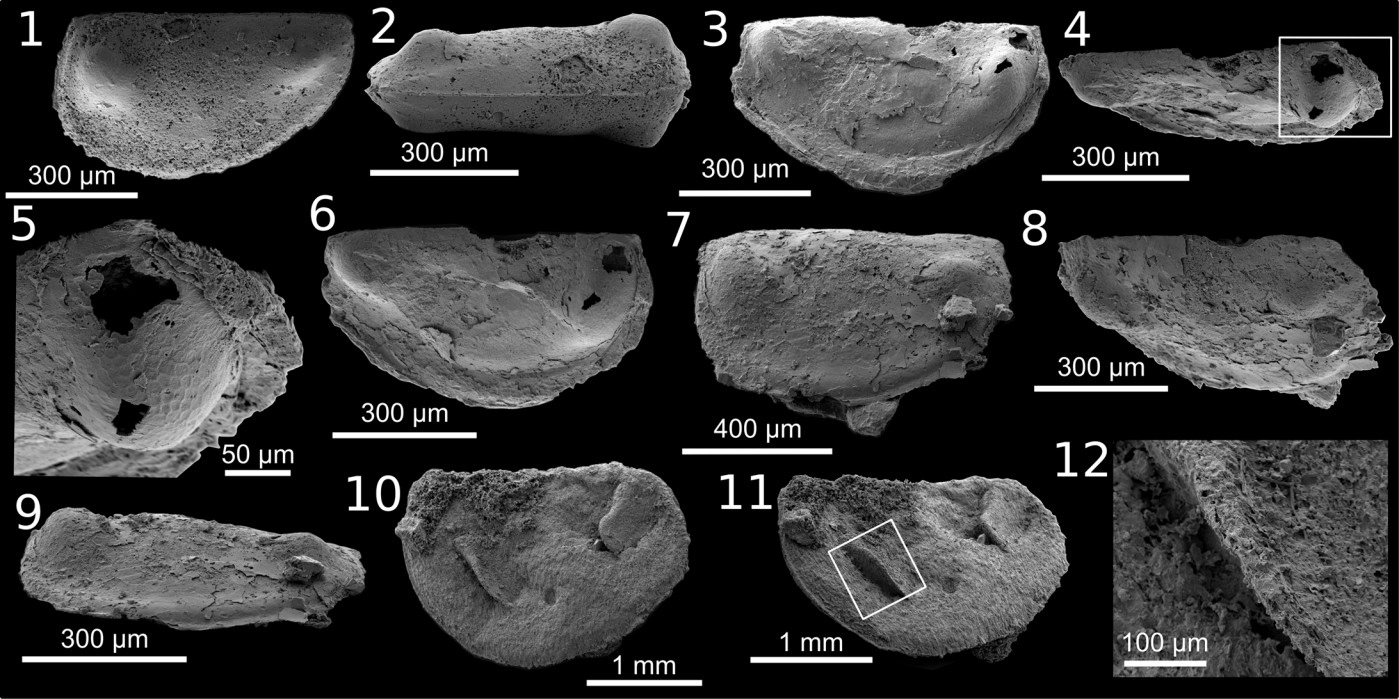
1
300 µm
2
300 µm
3
300 µm
4
300 µm
5
50 µm
6
300 µm
7
400 µm
8
300 µm
9
300 µm
10
1 mm
11
1 mm
12
100 µm

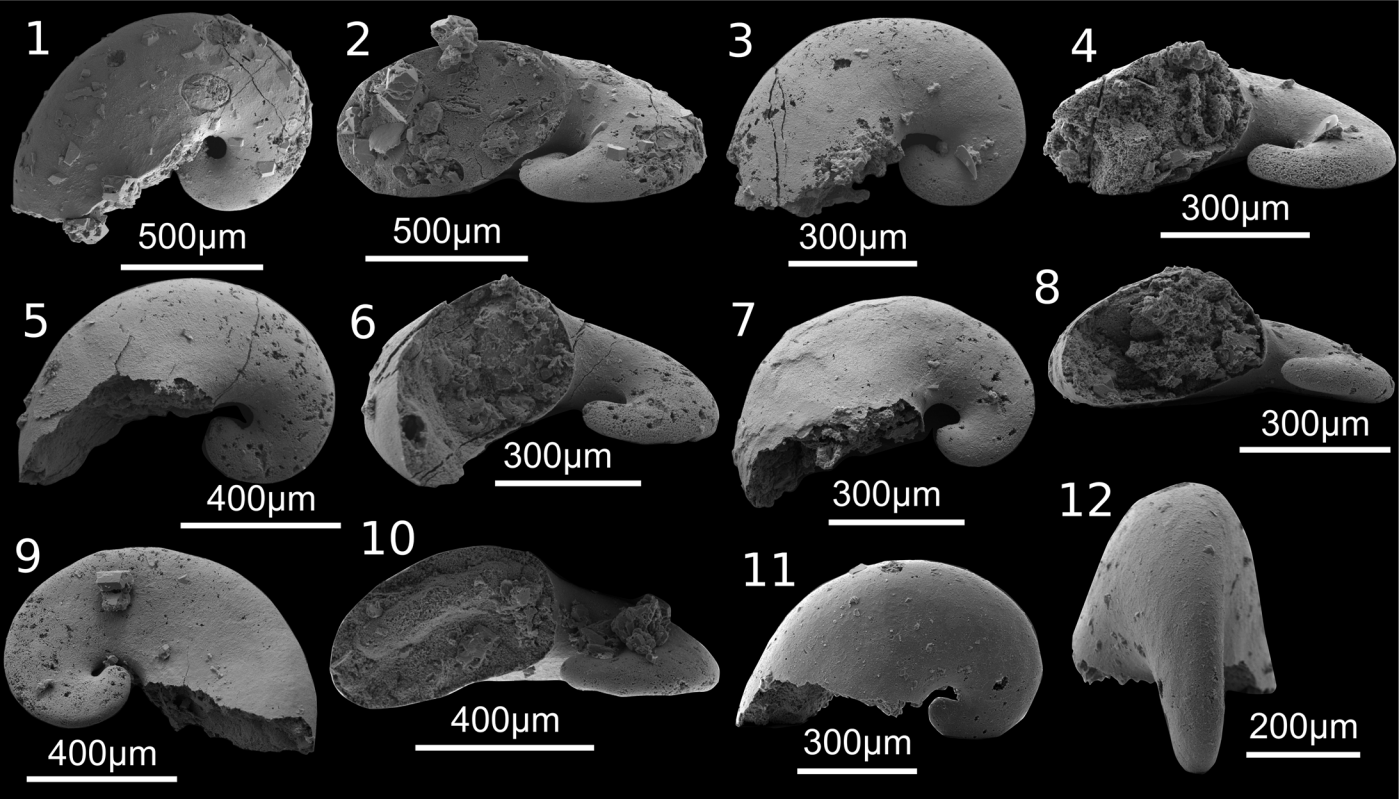
1
500µm
2
500µm
3
300µm
4
300µm
5
400µm
6
300µm
7
300µm
8
300µm
9
400µm
10
400µm
11
300µm
12
200µm

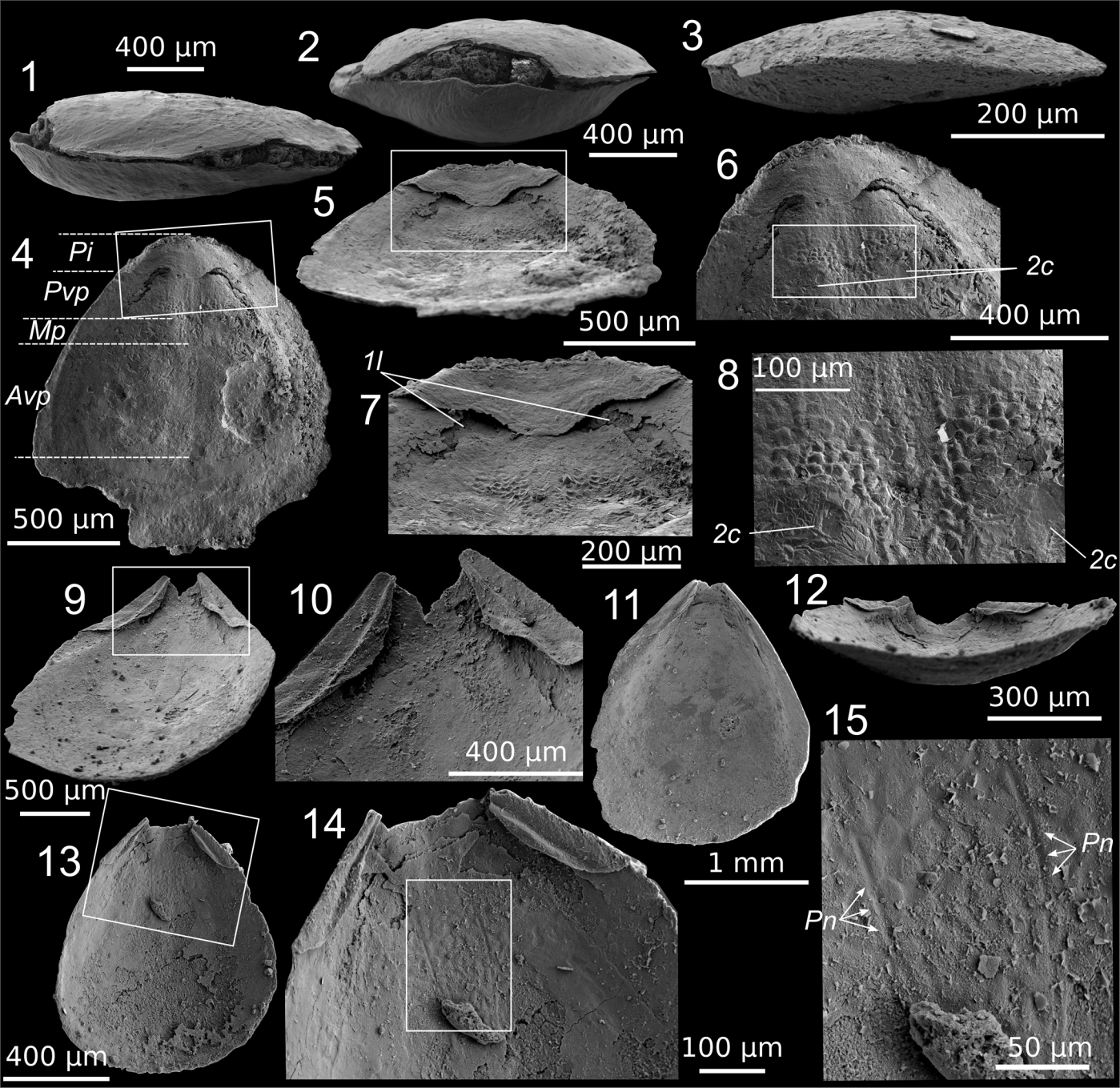
1
400 µm
2
400 µm
3
200 µm
4
Pi
Pvp
Mp
Avp
500 µm
5
500 µm
6
2c
400 µm
7
1l
200 µm
8
100 µm
2c
2c
9
500 µm
10
400 µm
11
1 mm
12
300 µm
13
400 µm
14
100 µm
15
Pn
Pn
50 µm

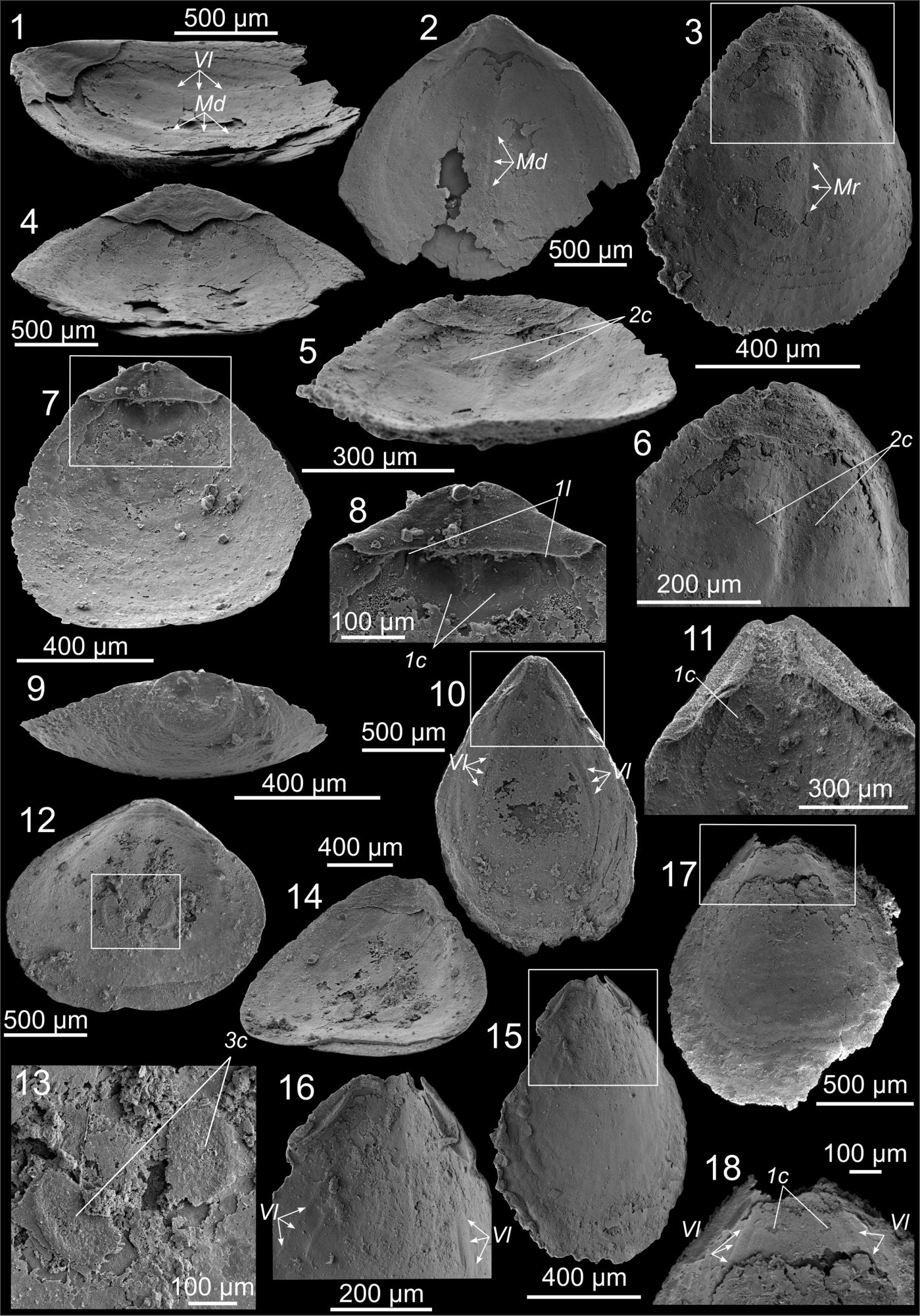
1
500 µm
Vl
Md
2
Md
500 µm
3
Mr
400 µm
4
500 µm
5
2c
300 µm
6
2c
200 µm
7
400 µm
8
1l
100 µm
1c
9
400 µm
10
500 µm
Vl
Vl
11
1c
300 µm
12
500 µm
400 µm
14
15
17
500 µm
3c
13
100 µm
16
Vl
Vl
200 µm
400 µm
18
100 µm
1c
Vl
Vl

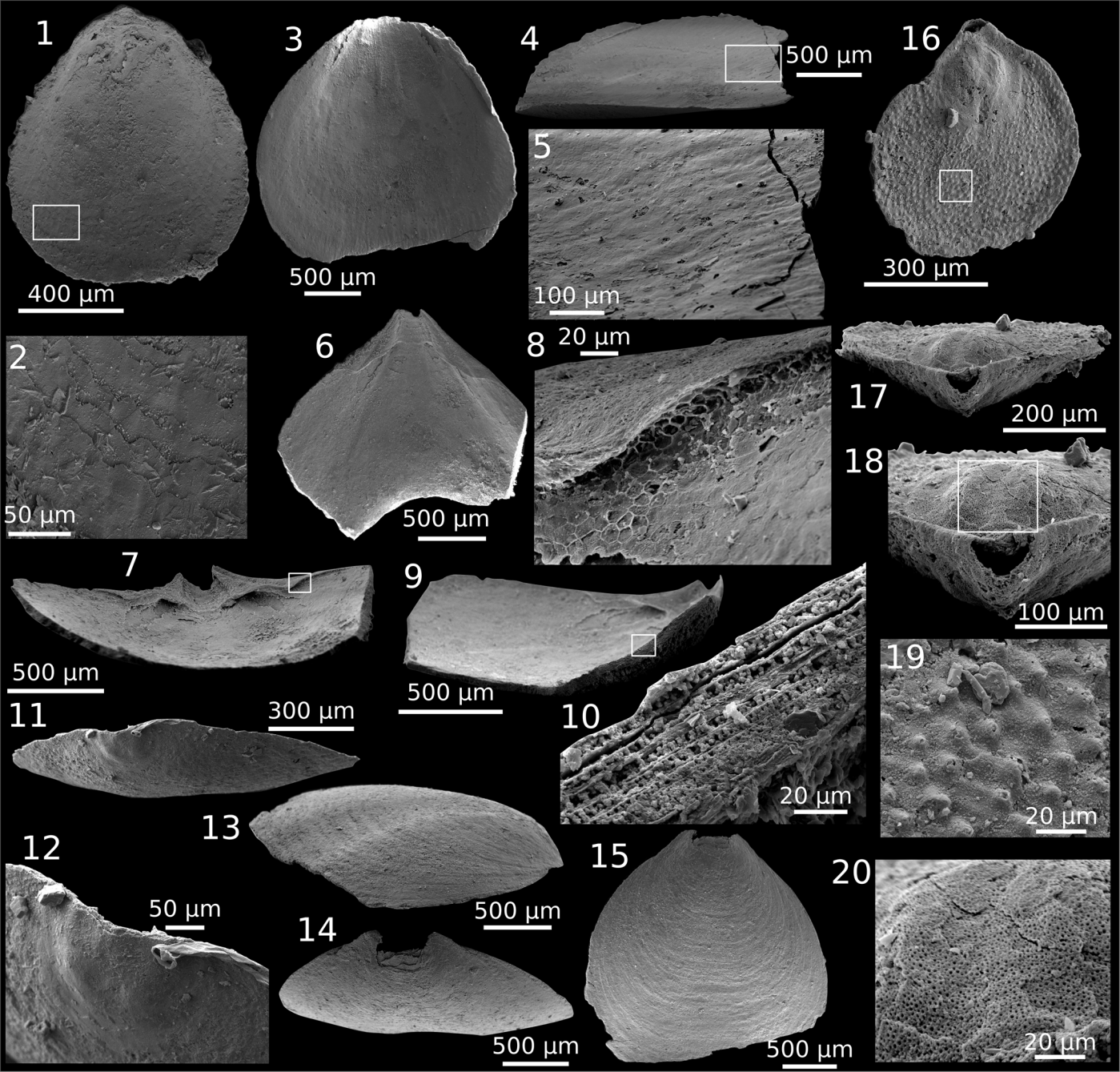
1
400 µm
3
500 µm
4
500 µm
16
300 µm
5
100 µm
2
50 µm
6
500 µm
8
20 µm
17
200 µm
18
100 µm
7
500 µm
9
500 µm
10
20 µm
19
20 µm
11
300 µm
13
500 µm
12
50 µm
14
500 µm
15
500 µm
20
20 µm

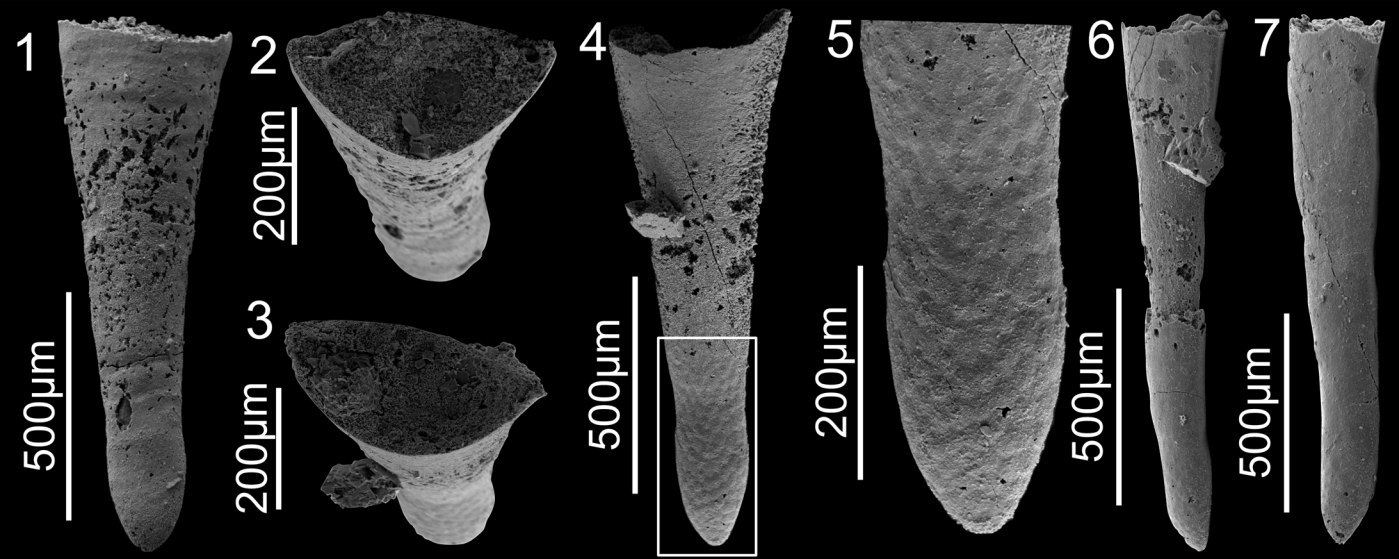
1
500µm
2
200µm
3
200µm
4
500µm
5
200µm
6
500µm
7
500µm

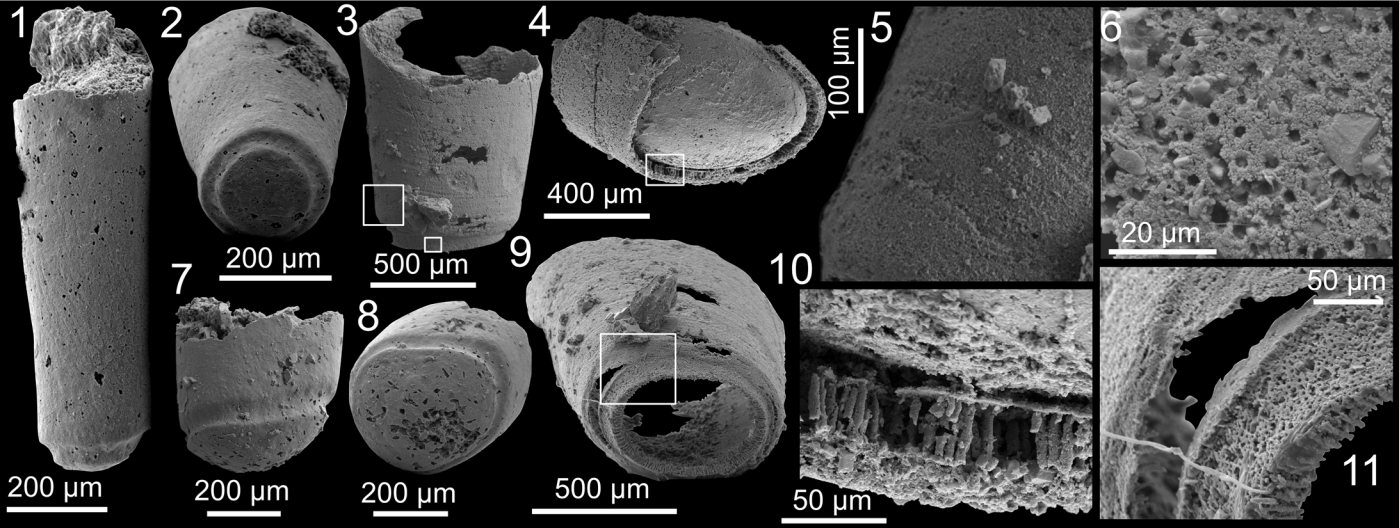
1
200 µm
2
200 µm
3
500 µm
4
400 µm
100 µm
5
6
20 µm
7
200 µm
8
200 µm
9
500 µm
10
50 µm
50 µm
11

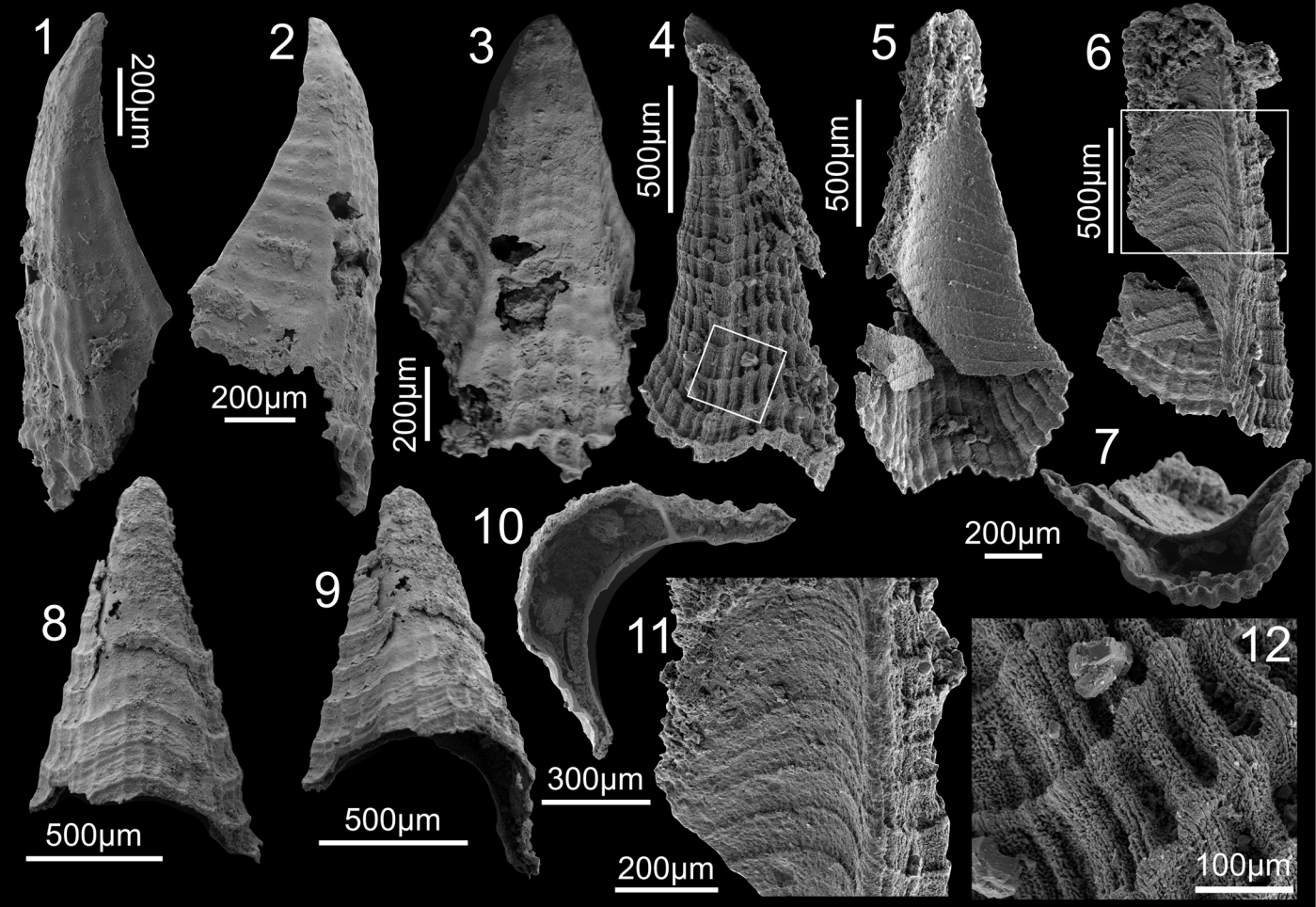
1
200μm
2
200μm
3
200μm
4
500μm
5
500μm
6
500μm
7
200μm
8
500μm
9
500μm
10
300μm
11
200μm
12
100μm

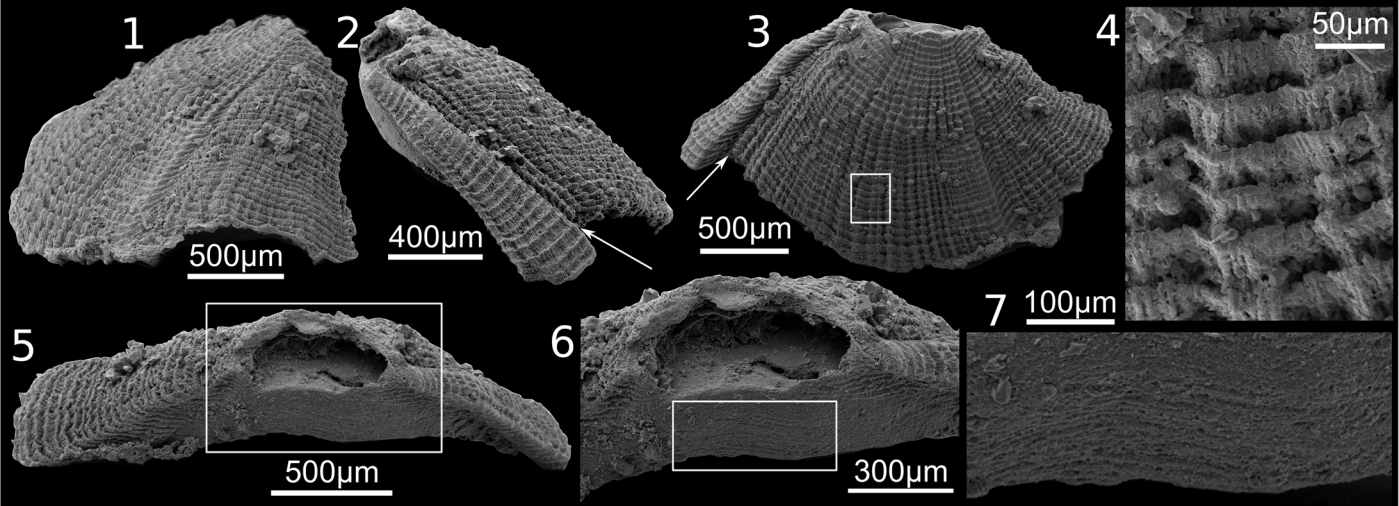
1
500µm
2
400µm
3
500µm
4
50µm
5
500µm
6
300µm
7
100µm

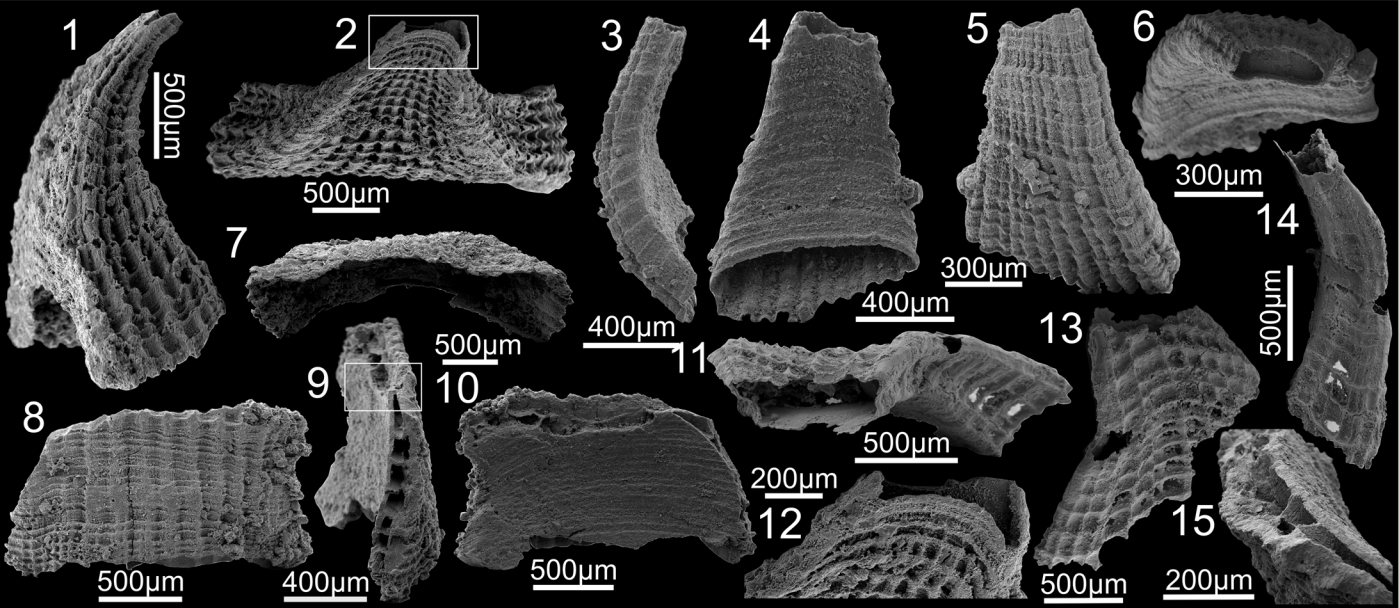
1
500µm
2
500µm
3
4
5
6
300µm
14
500µm
7
500µm
400µm
11
300µm
400µm
13
9
10
8
500µm
500µm
200µm
12
15
500µm
400µm
500µm
500µm
200µm

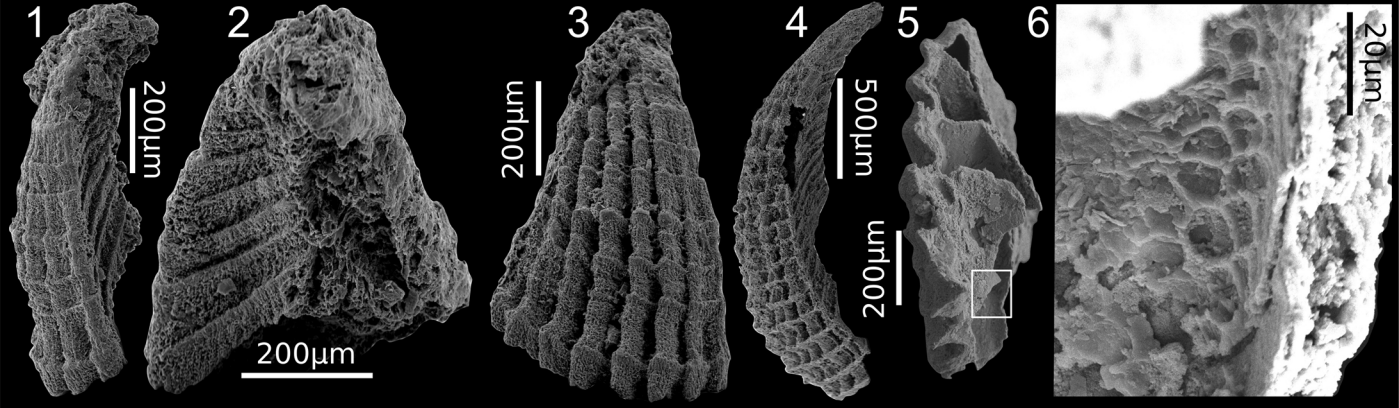
1
200µm
2
200µm
3
200µm
4
500µm
5
200µm
6
20µm

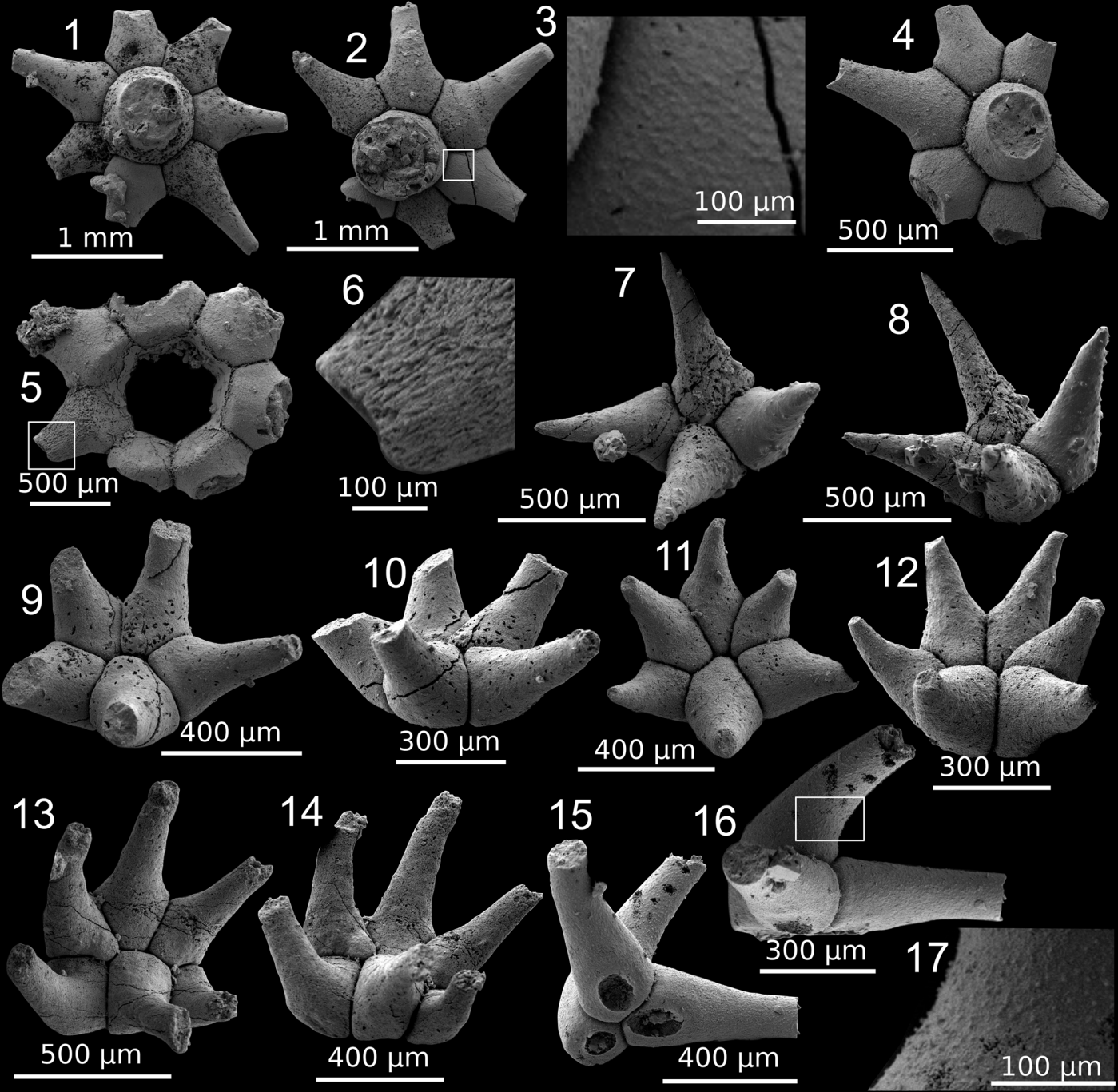
1
1 mm
2
1 mm
3
100 µm
4
500 µm
5
500 µm
6
100 µm
7
500 µm
8
500 µm
9
400 µm
10
300 µm
11
400 µm
12
300 µm
13
500 µm
14
400 µm
15
400 µm
16
300 µm
17
100 µm

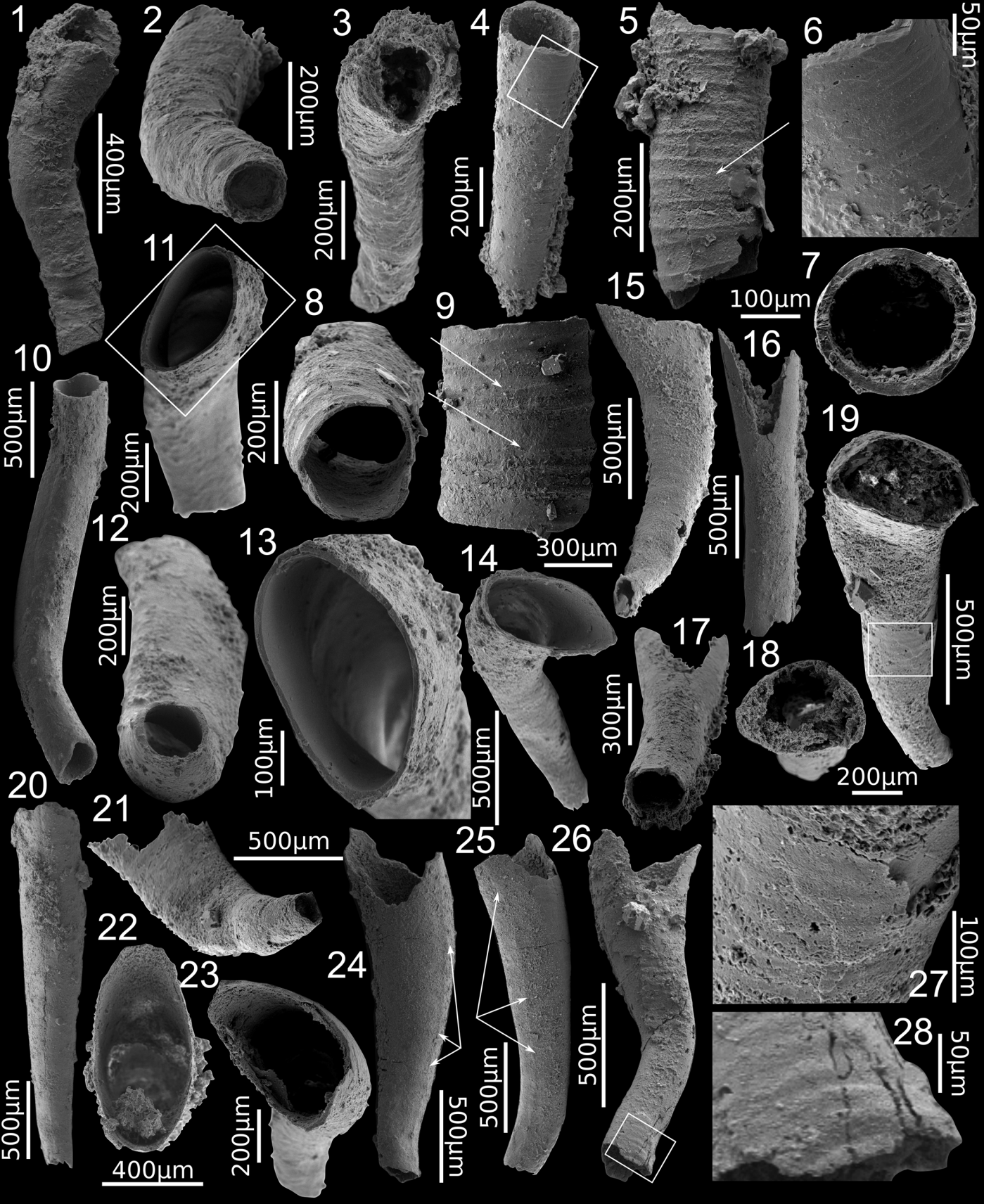
1
400µm
2
200µm
3
200µm
4
200µm
5
200µm
6
50µm
7
100µm
8
200µm
9
300µm
10
500µm
11
200µm
12
200µm
13
100µm
14
500µm
15
500µm
16
500µm
17
300µm
18
200µm
19
500µm
20
500µm
21
500µm
22
400µm
23
200µm
24
500µm
25
500µm
26
500µm
27
100µm
28
50µm

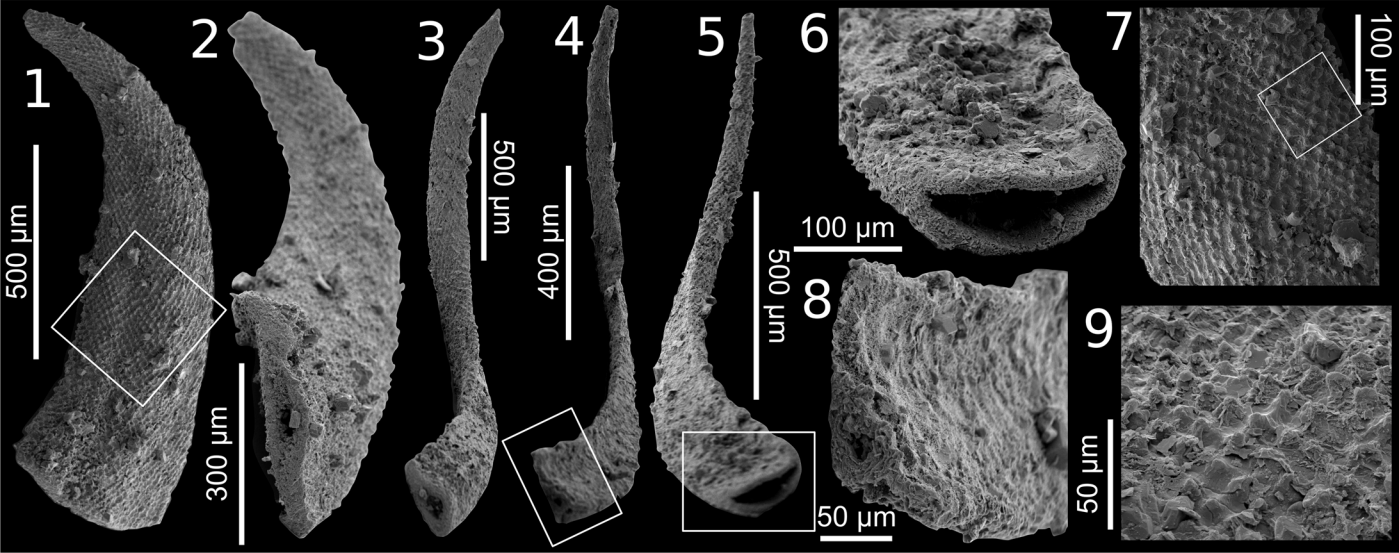
1
500 µm
2
300 µm
3
500 µm
4
400 µm
5
500 µm
6
100 µm
7
100 µm
8
50 µm
9
50 µm

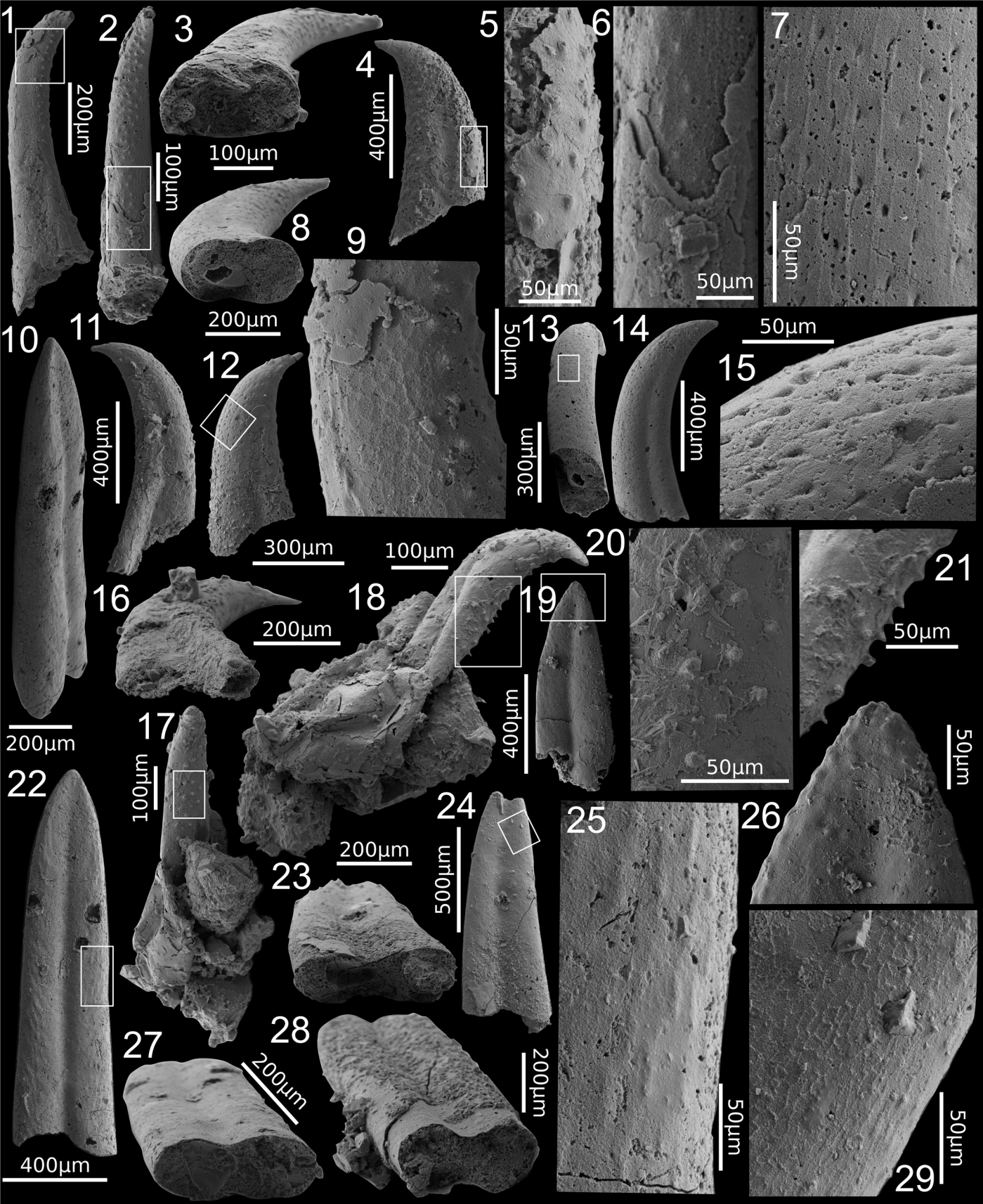
1
200µm
2
100µm
3
100µm
4
400µm
5
6
50µm
7
50µm
8
9
200µm
10
400µm
11
12
300µm
50µm
13
300µm
14
400µm
50µm
15
16
200µm
18
100µm
19
400µm
20
50µm
21
50µm
50µm
17
100µm
22
400µm
24
500µm
200µm
23
25
50µm
26
27
200µm
28
200µm
29
50µm